Stem Cell Reports
Article

OPEN ACCESS

Engineered Microenvironment for Manufacturing Human Pluripotent Stem Cell-Derived Vascular Smooth Muscle Cells

Haishuang Lin,[1,10] Xuefeng Qiu,[2,10] Qian Du,[3] Qiang Li,[1,4] Ou Wang,[1,4] Leonard Akert,[1] Zhanqi Wang,[5] Dirk Anderson,[6] Kan Liu,[3] Linxia Gu,[7] Chi Zhang,[3] and Yuguo Lei[1,4,8,9,*]

[1]Department of Chemical and Biomolecular Engineering, University of Nebraska-Lincoln, Lincoln, NE 68588, USA
[2]Department of Cardiovascular Surgery, Union Hospital, Tongji Medical College, Huazhong University of Science and Technology, Wuhan 430022, China
[3]Department of Biological Systems Engineering, University of Nebraska-Lincoln, Lincoln, NE 68588, USA
[4]Biomedical Engineering Program, University of Nebraska-Lincoln, Lincoln, NE 68588, USA
[5]Department of Vascular Surgery, Beijing Anzhen Hospital of Capital Medical University, Beijing Institute of Heart, Lung, and Blood Vessel Diseases, Beijing 100029, China
[6]Center for Biotechnology, University of Nebraska-Lincoln, Lincoln, NE 68588, USA
[7]Department of Mechanical and Materials Engineering, University of Nebraska-Lincoln, Lincoln, NE 68588, USA
[8]Mary and Dick Holland Regenerative Medicine Program, University of Nebraska Medical Center, Omaha, NE 68198, USA
[9]Fred & Pamela Buffett Cancer Center, University of Nebraska Medical Center, Omaha, NE 68198, USA
[10]Co-first author
*Correspondence: ylei14@unl.edu
https://doi.org/10.1016/j.stemcr.2018.11.009

SUMMARY

Human pluripotent stem cell-derived vascular smooth muscle cells (hPSC-VSMCs) are of great value for disease modeling, drug screening, cell therapies, and tissue engineering. However, producing a high quantity of hPSC-VSMCs with current cell culture technologies remains very challenging. Here, we report a scalable method for manufacturing hPSC-VSMCs in alginate hydrogel microtubes (i.e., AlgTubes), which protect cells from hydrodynamic stresses and limit cell mass to <400 μm to ensure efficient mass transport. The tubes provide cells a friendly microenvironment, leading to extremely high culture efficiency. We have shown that hPSC-VSMCs can be generated in 10 days with high viability, high purity, and high yield (~5.0×10^8 cells/mL). Phenotype and gene expression showed that VSMCs made in AlgTubes and VSMCs made in 2D cultures were similar overall. However, AlgTube-VSMCs had higher expression of genes related to vasculature development and angiogenesis, and 2D-VSMCs had higher expression of genes related to cell death and biosynthetic processes.

INTRODUCTION

Vascular smooth muscle cells (VSMCs) are critical in the development, function, and maintenance of blood vessels (Carmeliet, 2000; Owens et al., 2004). VSMC dysfunction can lead to a variety of diseases (Melanie et al., 2014; Porter and Riches, 2013). VSMCs are important, and required in large numbers for drug discovery and disease modeling (Biel et al., 2015; Ge et al., 2012; Granata et al., 2017; Ji et al., 2017; Kinnear et al., 2013a; Liu et al., 2011; Zhang et al., 2014, 2011), tissue engineering (Ferreira et al., 2007; Hibino et al., 2012; Karamariti et al., 2013; Levenberg, 2005; Park et al., 2010; Patsch et al., 2015; Wang et al., 2016, 2014; Yoo et al., 2013), and cell therapies (Cheung et al., 2012; Emilio et al., 2006; Hattan et al., 2004; Hong et al., 2017; Li et al., 1999; Matsubayashi et al., 2003; Staudacher et al., 2006; Wang et al., 2016; Wanjare et al., 2013; Ye et al., 2014). It is, however, a great challenge to retrieve enough primary VSMCs from fetal or adult human tissues (Cheung et al., 2014; Owens et al., 2004; Poh et al., 2005). This difficulty could potentially be resolved by using human pluripotent stem cells (hPSCs), including human embryonic stem cells (hESCs) (Thomson et al., 1998) and induced pluripotent stem cells (iPSCs) (Levenberg et al., 2007; Takahashi et al., 2007; Yu et al., 2007). Large numbers of hPSCs can be grown due to their ability to continually proliferate *in vitro*. They are also capable of differentiating into all somatic cell types (Chen et al., 2011; Lei and Schaffer, 2013). Also, patient-specific derived iPSCs retain the patient's genetic information, which is important in modeling many human diseases (Okita et al., 2011; Takahashi et al., 2007). This also allows these cells to produce little or no immune response in the patient (Lalit et al., 2014). Protocols for effectively differentiating hPSCs into VSMCs have been developed in the past decade, through either embryoid bodies (Biel et al., 2015; Ge et al., 2012; Kinnear et al., 2013b; Lee et al., 2010; Lin et al., 2012; Wang et al., 2014; Yoo et al., 2013; Zhang et al., 2014) or monolayer culture (Bajpai et al., 2012; Bao et al., 2015; Cheung et al., 2012; Karamariti et al., 2013; Lian et al., 2014; Liu et al., 2011; Melanie et al., 2014; Park et al., 2010; Patsch et al., 2015; Taura et al., 2009; Wanjare et al., 2015, 2013; Yang et al., 2016; Zhang et al., 2011). For instance, researchers are able to generate developmental origin-specific VSMC subtypes from hPSCs, including neuroectodermal VSMCs, lateral plate mesodermal VSMCs, and paraxial mesodermal VSMCs (Bernardo et al., 2011; Cheung et al., 2012; Granata et al., 2017; Iyer et al., 2016; Raphel et al., 2012; Sinha et al., 2004), or synthetic (Granata et al., 2017; Wanjare et al., 2013, 2015) and contractile

VSMCs from hPSCs (Bajpai et al., 2012; Eoh et al., 2017; Gerecht et al., 2010; Patsch et al., 2015; Pei et al., 2010; Vo et al., 2010; Wanjare et al., 2015; Yang et al., 2016). Synthetic VSMCs are at a proliferative state, while contractile VSMCs are at a quiescent yet functional state (Ayoubi et al., 2017). Contractile VSMCs are critical for maintaining proper blood flow and normal vessel tone (Alexander and Owens, 2012). The synthetic phenotype has an unfavorable role in human blood vessels, and is associated with conditions such as atherosclerosis and hypertension (Lacolley et al., 2012; Louis and Zahradka, 2010). Under certain conditions, VSMCs can actually switch between the two phenotypes (Mark and Christine, 2012). Patsch and colleagues have recently demonstrated a protocol that can differentiate hPSCs into mesoderm and then VSMCs, using a two-dimensional (2D) culture system, in just 6 days (Patsch et al., 2015). Their protocol is efficient and simple, making it incredibly useful for making VSMCs for a range of biomedical procedures, especially for clinical applications.

Although it is possible to readily make hPSC-VSMCs on a small scale in basic research laboratories, it is still very difficult to produce hPSC-VSMCs at the larger quantities needed by many biomedical applications. The current 2D methods for culturing cells (e.g., growing cells on 2D surfaces like plates or flasks) generally produce such a low cell yield that they are typically utilized when small numbers of cells are needed (e.g., $<10^{10}$) (Jenkins and Farid, 2015; Kropp et al., 2017). Three-dimensional suspension culturing methods (e.g., culturing cells in agitated medium in stirred-tank bioreactors) are being studied to scale up the cell production, and this technique has been shown to have encouraging results. However, 3D culture systems do have significant limitations (Jenkins and Farid, 2015; Kropp et al., 2017; Lei et al., 2014; Lei and Schaffer, 2013; Serra et al., 2012; Steiner et al., 2010; Wurm, 2004). hPSCs have both strong cell-to-cell and strong cell-to-matrix adhesions. They frequently form large cellular agglomerates by aggregating in 3D suspension (Kropp et al., 2017). Due to the fact that the diffusion limit in human tissue is in the range of 300–400 μm, the mass transport in cellular agglomerates larger than 400 μm (in diameter) becomes limited. This restriction in mass transport can increase apoptosis, cause uncontrolled differentiation, and slow cell growth (Kropp et al., 2017). Mass transport and medium mixing can be enhanced, and cell agglomeration can be reduced by simply agitating the culture. While agitation has its benefits, it can also generate significant, negative, and uncontrollable hydrodynamic stresses (e.g., shear force), which can greatly increase cell death (Fridley et al., 2012; Kinney et al., 2011; Kropp et al., 2017). This can result in decreased cell viability leading to slower growth and lower volumetric yield, all of which are common in 3D suspension culturing (Lei and Schaffer, 2013).

To address the challenge, we previously developed a scalable and high-yield cell culture method for expanding hPSCs and other human cells (Li et al., 2018a, 2018b; Lin et al., 2018a, 2018b). With this method, cells are processed into microscale alginate hydrogel tubes (AlgTubes) that are suspended in the cell culture medium. These tubes significantly improved the hPSC culture efficiency and consistency. Under optimized culture conditions, hPSCs could be cultured in these hydrogel tubes long term (e.g., >10 passages, >50 days) with high cell viability, high purity (>95% pluripotency markers, e.g., *OCT4*, *NANOG*, *ALP*, and *SSEA4*), and high yield (~5.0×10^8 cells/mL of microspace). However, whether hPSCs can be efficiently differentiated into VSMCs in the alginate hydrogel tubes and if alginate hydrogel tubes could affect the phenotypes of produced VSMCs have not been studied. In this paper, we systematically address these questions. Consequently, we have developed a highly efficient and scalable method for producing hPSC-VSMCs with high volumetric yield, high viability, and high purity.

RESULTS

Processing Cells into Alginate Hydrogel Tubes

A microextruder was used to process hPSCs into AlgTubes according to our previous study (Li et al., 2018a) (Figures 1A–1C). In the hydrogel tubes, single hPSCs first associated to form small clusters that subsequently grew into spheroids that eventually filled the tube (Figure 1D). Very few dead cells were detected during the culture (Figure 1E). Immunostaining and flow cytometry analyses revealed >95% cells positive for the pluripotency markers *OCT4*, *NANOG*, *ALP*, and *SSEA4* (Figure 1F). When seeded at 1.0×10^6 cells/mL, H9s, Fib-iPSCs (iPSCs reprogrammed from dermal fibroblasts), and MSC-iPSCs (iPSCs reprogrammed from bone marrow mesenchymal stem cells) expanded ~30-, ~150-, and ~480-fold to yield ~30, 150, and 480×10^6 cells/mL of microspace on days 5, 7, and 9, respectively (Figures 1G and 1H). For comparison, typically 2–3 million cells can be generated in one well of a six-well plate. To generate massive numbers of hPSCs, the day 9 cell masses can be released by dissolving the hydrogel tubes with 0.5 mM EDTA solution (5 min at room temperature), and dissociated into single cells with Accutase and processed into new hydrogel tubes for a second round of expansion. Once the targeted cell number is reached, hPSCs can be differentiated into VSMCs within 5 days.

Making hPSC-VSMCs in Alginate Hydrogel Tubes

We first checked and confirmed that our starting cells, including H9 hESCs, Fib-iPSCs, and MSC-iPSCs (Park et al., 2008), were high-quality pluripotent stem cells

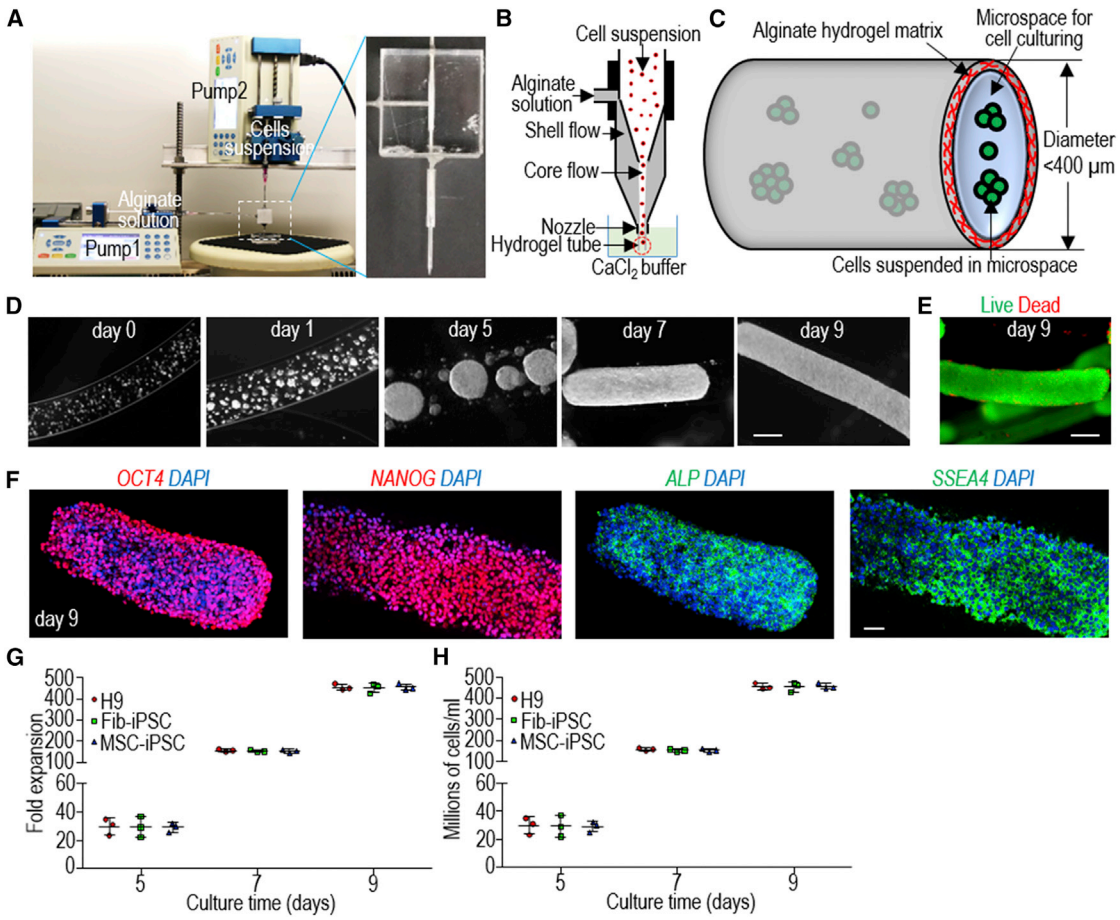

Figure 1. Culturing hPSCs in Alginate Hydrogel Tubes (AlgTubes)

(A–C) Overview of alginate hydrogel culture system. (A) A microextruder is built for processing cells into microscale alginate hydrogel tubes. (B) A cell suspension and an alginate solution are pumped into the central channel and side channel of the microextruder, respectively, to form coaxial core-shell flows that are extruded through the nozzle into a $CaCl_2$ buffer. (C) The hydrogel tubes protect cells from hydrodynamic stresses and confine the cell mass to <400 μm (in radial diameter) to ensure efficient mass transport. The tubes provide uniform and cell-friendly microspaces that allow cells to interact with one another and expand.

(D) Phase images of H9 hESCs in hydrogel tubes on days 0, 1, 5, 7, and 9. Scale bar, 200 μm.

(E) Live/dead cell staining of day 9 cells in hydrogel tubes. Scale bar, 200 μm.

(F) Immunostaining of day 9 H9 hESCs for pluripotency markers *OCT4*, *NANOG*, *SSEA4*, and *ALP*. Scale bar, 200 μm.

(G and H) Seeded at 1.0 × 10^6 cells/mL, H9s, Fib-iPSCs, and MSC-iPSCs expanded (G) ~30-, 150-, and 480-fold to yield (H) ~30, 150, and 480 × 10^6 cells/mL of microspace on days 5, 7, and 9. Data are represented as mean ± SD (n = 3).

(Figure S1). Patsch et al. reported an efficient protocol that could differentiate hPSCs into VSMCs in 6 days in 2D culturing (Patsch et al., 2015). This protocol is simple and quick, and thus is very appealing for making VSMCs for various biomedical applications, especially for clinical applications. We successfully repeated this protocol (Figure S2). We termed VSMCs made in 2D culturing as 2D-VSMCs.

We then studied whether the protocol could be used to generate VSMCs in alginate hydrogel tubes (Figure 2A). Single hPSCs were processed into the hydrogel tubes and expanded for 5 days to generate small spheroids. On day 5, the differentiation medium was applied. Cells were harvested for analysis on day 10 (Figure 2B). Live/dead staining and cell viability analysis showed very high cell viability on day 10 (Figures 2C and 2D). About 5.0 × 10^8 cells/mL of microspace were produced on day 10 (Figure 2E). Immunostaining and confocal imaging showed that the majority of the produced cells were positive for VSMC markers *SM22A* and *α-SMA* (Figures 2F and 2G). VSMCs were uniformly distributed, and no cysts were found in the cell mass, indicating no or little cell death

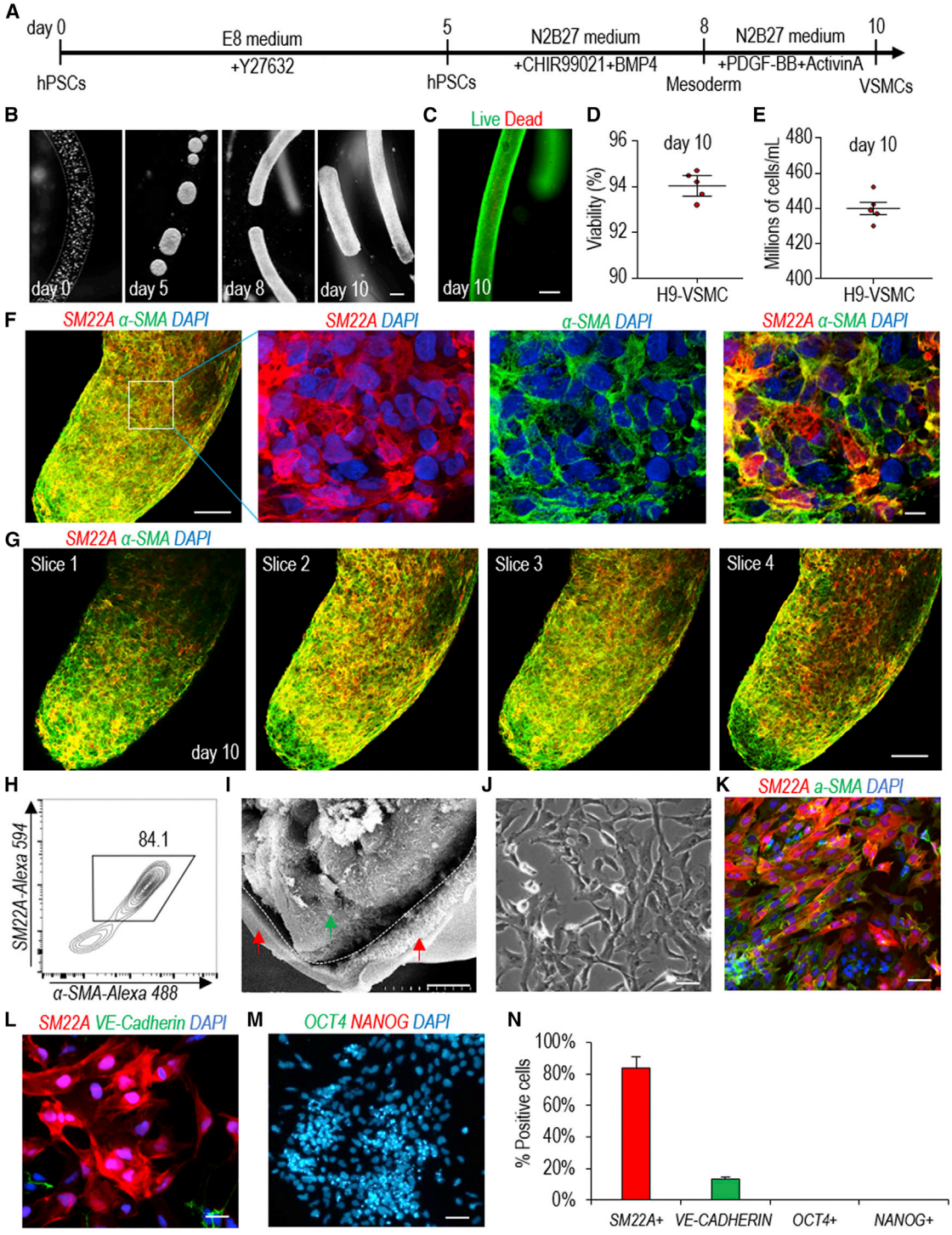

Figure 2. Differentiating H9 hESCs into VSMCs in Alginate Hydrogel Tubes

(A) The VSMC differentiation protocol.

(B) Phase images of day 0, 5, 8, and 10 cells. Scale bar, 200 μm.

(C and D) (C) Live/dead staining and (D) cell viability of day 10 cells. Data are represented as mean ± SD (n = 5). Scale bar, 200 μm.

(E) Volumetric yield on day 10. Data are represented as mean ± SD (n = 5).

(legend continued on next page)

during the differentiation. Flow cytometry analysis found 84.1% of the cells were *SM22A*+ and *α-SMA*+ (Figure 2H). Scanning electron microscopy (SEM) showed there was no adhesion between AlgTube-VSMCs and alginate hydrogel tubes (Figure 2I). When the day 10 cells were released from the tubes and dissociated into single cells and plated on Matrigel-coated plates at high density, they formed a monolayer with tight cell-cell interactions (Figure 2J). The majority of the cells were *SM22A*+ and *α-SMA*+ VSMCs (Figure 2K), ~10% of cells were *VE-CADHERIN*+ endothelial cells (Figures 2L and 2N), and no *OCT4*+ and *NANOG*+ undifferentiated hPSCs were detected (Figures 2M and 2N). H9s, Fib-iPSCs, and MSC-iPSCs had similar outcomes (Figures S3 and S4). We found that the differentiation efficiencies in 2D culturing and in hydrogel tubes were very close. We termed VSMCs made in hydrogel tubes as AlgTube-VSMCs.

To study whether the diameter of the hydrogel tubes affected the differentiation efficiency, we differentiated hPSCs into VSMCs in hydrogel tubes with a diameter of 120, 250, or 330 μm. The diameter of the hydrogel tubes can be precisely controlled through adjusting the nozzle diameter of the microextruder (Li et al., 2018a). hPSCs were successfully differentiated into VSMCs in all three tubes with similar cell viability, differentiation efficiency, and yield (Figures S5A and S5B). Quantitative RT-PCR analysis revealed that cells in 250 μm hydrogel tubes had significantly higher expression for some important VSMC genes, including *α-SMA*, *SM22A*, *CALPONIN*, *VEGFA*, *FN*, *COL4A5*, and *COL4A6* (Figures S5C–S5E). We thus decided to use 250 μm hydrogel tubes for the rest of the studies.

Properties of hPSC-VSMCs Made in Alginate Hydrogel Tubes and 2D Culture

Our culture system provides cells a 3D microenvironment. Recent research on organoids demonstrates that 3D microenvironments promote the formation of structured tissues during the differentiation of pluripotent stem cells (Hattori, 2014; Jo et al., 2016; Takahashi et al., 2018). Therefore, we asked if AlgTube-VSMCs and 2D-VSMCs were similar in phenotypes, functions, and gene expression. VSMCs were replated in six-well plates for phenotype assays after 5 days differentiation. The fibronectin deposition assay showed that AlgTube-VSMCs and 2D-VSMCs had similar fibronectin production in response to transforming growth factor β (TGF-β) stimulation (Figures 3A–3C). When co-cultured with human umbilical vein endothelial cells (HUVECs), both types of VSMCs attached to the tubular network formed by the HUVECs (Figure 3D). AlgTube-VSMCs had more contraction in response to carbachol treatment than 2D-VSMCs *in vitro* (Figures 3E–3G), although the carbachol-induced intracellular calcium levels were similar (Figure 3H). When subcutaneously injected with HUVECs into immunodeficient mice for 2 weeks, both AlgTube-VSMCs and 2D-VSMCs contributed to the newly formed blood vessels (Figure 3I). The numbers of VSMCs attached to the vessels were similar (Figure 3J). Similar results were found for Fib-iPSC-derived VSMCs (Figures S6A–S6G). These results show that AlgTube-VSMCs and 2D-VSMCs are similar and both have the typical VSMC phenotypes.

Transcriptome Analysis of AlgTube-VSMCs and 2D-VSMCs

We sequenced the mRNAs of AlgTube-VSMCs and 2D-VSMCs derived from H9s and undifferentiated H9s (three biological replicates for each) to analyze their global gene expression. Hierarchical clustering analysis showed that AlgTube-VSMCs and 2D-VSMCs clustered closely (Figure 4A). The genome-wide gene expression profile correlation coefficients between the AlgTube-VSMCs and the 2D-VSMCs were >0.81, indicating that they had similar global gene expressions (Figure 4B). However, the separation of 2D-VSMCs and AlgTube-VSMCs in PC2 of the principal component analysis (PCA) indicated these cells had some differences in gene expression (Figure 4C), which drove us to perform differential gene expression analysis.

Differential gene expression analysis identified 807 genes significantly upregulated in AlgTube-VSMCs, and 719 genes significantly upregulated in 2D-VSMCs (Table S3). Gene Ontology (GO) terms upregulated in AlgTube-VSMCs were mainly related to vasculature development and angiogenesis (Figure 4D). GO terms upregulated in 2D-VSMCs were related to apoptotic process and biosynthesis (Figure 4E). Detailed gene expression analysis using the RNA sequencing (RNA-seq) data showed that AlgTube-VSMCs and 2D-VSMCs had significant differences in the expression of genes related to extracellular matrices, such as those for *COLLAGENS*, *LAMININS*, *INTEGRINS*, and *PROTEASES* (Figures S7A–S7E); VSMC secreted factors (Figure S7F); *EPHRIN* signaling (Figure S7G); angiogenesis

(F–H) (F) Immunostaining and (H) flow cytometry analysis of day 10 cells for VSMC markers *SM22A* and *α-SMA*. (G) Confocal microscope images of four slices of one fibrous cell mass stained with VSMC markers *α-SMA* and *SM22A*. Scale bars, 100 and 10 μm, respectively.
(I) SEM image of hPSC-VSMCs in hydrogel tubes on day 10 (green arrow, cells; red arrows, hydrogel tubes). Scale bar, 10 μm.
(J–N) The day 10 cell masses were dissociated into single cells and plated on 2D surface overnight. (J) Phase image and (K) immunostaining showed the majority of the cells were *SM22A*+ and *α-SMA*+ VSMCs, and (L and N) ~10% were *VE-CADHERIN*+ endothelial cells, but (M and N) there were no *OCT4+/NANOG*+ undifferentiated hPSCs. Data are represented as mean ± SD (n = 3). Scale bar, 50 μm.

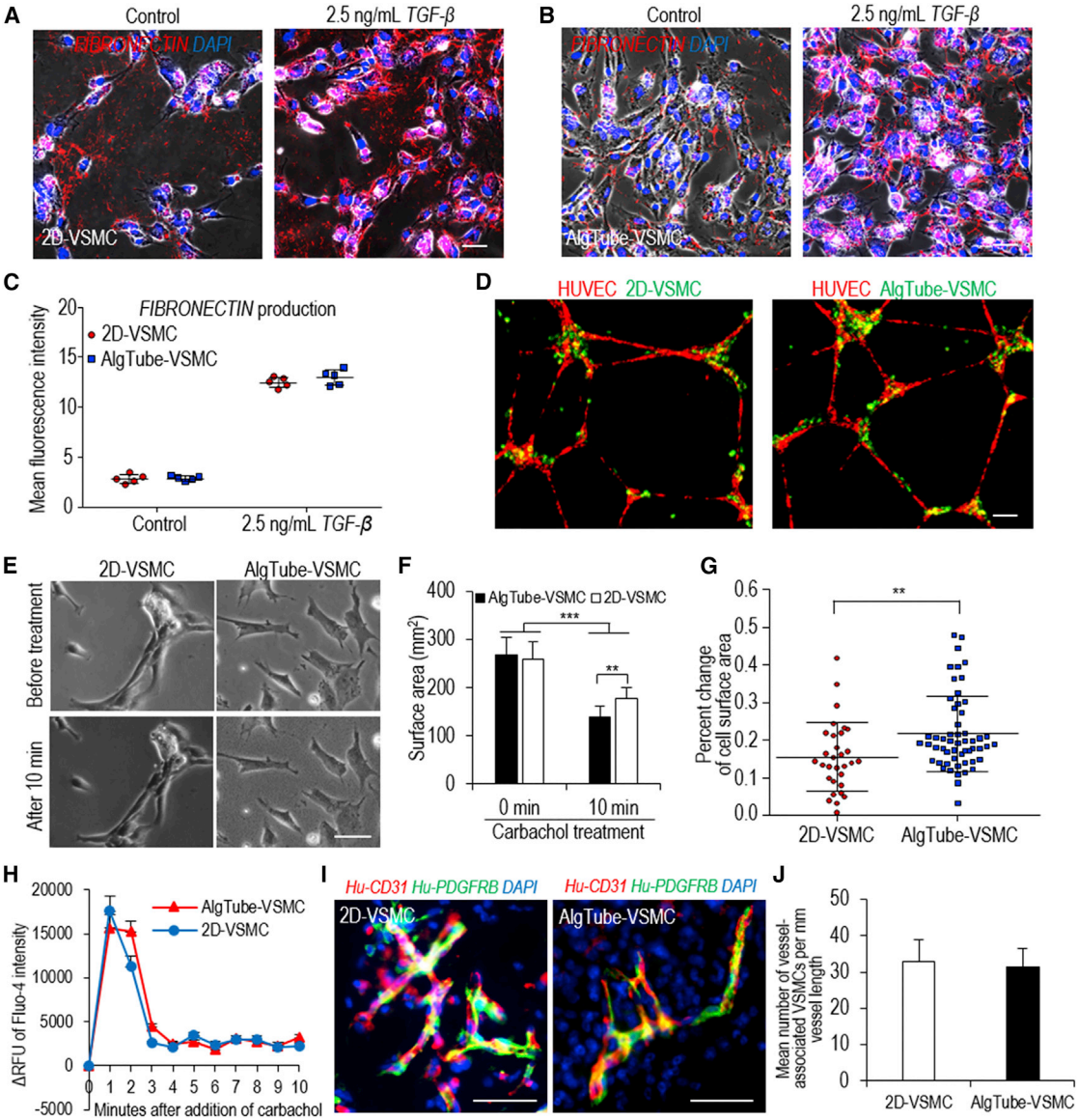

Figure 3. Properties of hPSC-VSMCs Made in 2D Culture (2D-VSMCs) and Alginate Hydrogel Tubes (AlgTube-VSMCs)

(A–C) Immunostaining of fibronectin production of (A) 2D-VSMCs and (B) AlgTube-VSMCs after 24 hr of 2.5 ng/mL TGF-β treatment. (C) Quantification of produced fibronectin. Data are represented as mean ± SD (n = 5). Scale bar, 50 μm.

(D) Co-culture of VSMCs and HUVECs. Scale bar, 50 μm.

(E–G) (E) Phase images, (F) surface area, and (G) percentage change in cell surface area of 2D-VSMCs and AlgTube-VSMCs in response to carbachol treatment. Data are represented as mean ± SD. **$p < 0.01$, ***$p < 0.001$. Scale bar, 50 μm.

(H) The relative fluorescence units (ΔRFU) of Fluo-4-loaded VSMCs over 10 min after adding carbachol. Data are represented as mean ± SD (n = 3).

(I and J) When VSMCs and HUVECs were co-transplanted subcutaneously, both 2D-VSMCs and AlgTube-VSMCs (I) formed nice vascular structures with (J) similar numbers of VSMCs attached to the vessels. Scale bar, 50 μm.

(Figure S7H); vasculature development (Figure S7I); *NOTCH* signaling (Figure S7J); cell differentiation (Figure S7K); and cell cycle and proliferation (Figure S7L). These results show that the 3D microenvironment of AlgTubes promoted vasculature development during the differentiation.

We also briefly compared the global gene expression profiles of AlgTube-VSMCs and 2D-VSMCs with those of

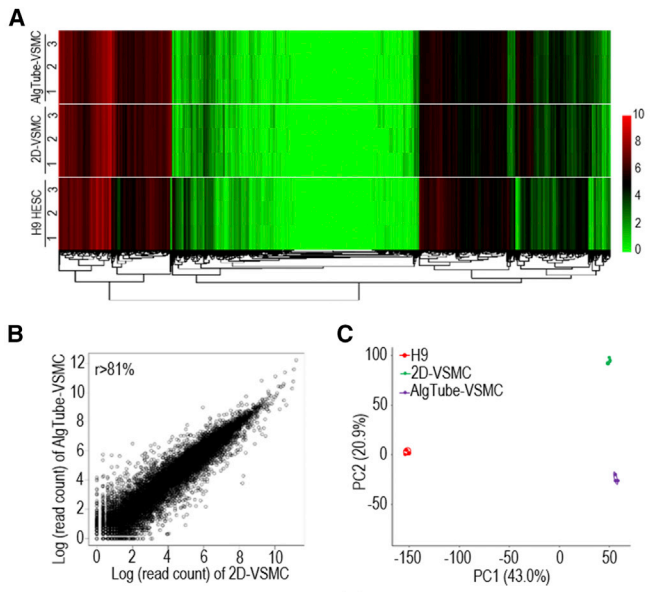

D

Top 20 upregulated GO terms in AlgTube-VSMCs

GO ID	GO term	P value
GO:0048731	system development	5.34E-19
GO:0001944	**vasculature development**	1.06E-17
GO:0001568	**blood vessel development**	1.13E-17
GO:0048514	**blood vessel morphogenesis**	1.92E-17
GO:0072358	**cardiovascular system development**	2.68E-17
GO:0071310	cellular response to organic substance	2.73E-16
GO:0001525	**angiogenesis**	4.71E-16
GO:0072359	**circulatory system development**	1.55E-15
GO:0007166	**cell surface receptor signaling pathway**	1.29E-12
GO:0016477	**cell migration**	1.32E-12
GO:0048513	animal organ development	1.62E-12
GO:0034097	response to cytokine	3.36E-11
GO:0030154	**cell differentiation**	8.06E-11
GO:0006355	regulation of transcription, DNA-templated	1.17E-10
GO:0048870	**cell motility**	1.26E-10
GO:0001501	**skeletal system development**	2.16E-10
GO:1903506	regulation of nucleic acid-templated transcription	2.2E-10
GO:0035556	intracellular signal transduction	2.91E-10
GO:0006468	protein phosphorylation	3.05E-10
GO:0030334	regulation of cell migration	5.02E-10

E

Top 20 upregulated GO terms in 2D-VSMCs

GO ID	GO term	P value
GO:0006915	**apoptotic process**	2.06E-16
GO:0012501	**programmed cell death**	3.84E-15
GO:0042981	regulation of apoptotic process	1.57E-14
GO:0043067	regulation of programmed cell death	3.16E-14
GO:0048731	system development	1.86E-13
GO:0044283	small molecule biosynthetic process	2.66E-13
GO:0071310	cellular response to organic substance	7.49E-10
GO:0060548	negative regulation of cell death	1.34E-09
GO:0043066	negative regulation of apoptotic process	1.69E-09
GO:0006694	steroid biosynthetic process	1.98E-09
GO:0048513	animal organ development	2.44E-09
GO:0036293	response to decreased oxygen levels	2.63E-09
GO:0043069	negative regulation of programmed cell death	3.33E-09
GO:0035556	intracellular signal transduction	5.94E-09
GO:1901617	organic hydroxy compound biosynthetic process	7.15E-09
GO:0016126	sterol biosynthetic process	7.79E-09
GO:1901701	cellular response to oxygen-containing compound	7.98E-09
GO:0008203	cholesterol metabolic process	8.05E-09
GO:0097190	**apoptotic signaling pathway**	9.61E-09
GO:0008284	**positive regulation of cell proliferation**	1.49E-08

Figure 4. Whole Transcriptome Analysis of AlgTube-VSMCs and 2D-VSMCs Derived from H9 hESCs

(A) Global heatmap of expressed genes.

(B) The scatterplot in log scale of global gene expression between AlgTube-VSMCs and 2D-VSMCs.

(C) Principal component analysis of AlgTube-VSMCs, 2D-VSMCs, and H9s. Three biological replicates were used for each sample.

(D and E) Top 20 GO terms of upregulated genes in (D) AlgTube-VSMCs and (E) 2D-VSMCs.

primary human aortic smooth muscle cells (HASMCs). The RNA-seq data of primary HASMCs were obtained from the literature (Pan et al., 2018). It should be noted that these HASMCs had been cultured in 2D plates in serum-containing medium before RNA sequencing and the 2D culturing may have altered their global gene expression profiles. The genome-wide gene expression profile correlation coefficients were 0.74 between AlgTube-VSMCs and HASMCs, and were 0.63 between 2D-VSMCs and HASMCs (Figures S7M and S7N). These results indicate that AlgTube-VSMCs are closer to HASMCs than 2D-VSMCs. However, both AlgTube-VSMCs and 2D-VSMCs have differences from HASMCs in terms of global gene expression. It is likely due to the fact that VSMCs derived from hPSCs are not as mature as primary VSMCs. Further studies to identify the differences in gene expression, phenotypes, and functions between hPSC-VSMCs and primary VSMCs (especially those that have not been cultured *in vitro*) should be done in the future.

Using quantitative RT-PCR analysis, we found that both AlgTube-VSMCs and 2D-VSMCs had very low expression levels of the pluripotency markers *OCT4* and *NANOG* (Figure 5A). 2D-VSMCs had higher expression of the synthetic VSMC genes such as *α-SMA*, *SM22A*, and *CALPONIN* (Figure 5B), and AlgTube-VSMCs had higher expression of the mature and contractile VSMC markers such as *SMOOTHELIN* (*SMTN*), *MYOSIN HEAVY CHAIN 11* (*MYH11*), and *ELASTIN* (Figure 5C). These results indicate that 2D-VSMCs are closer to a synthetic phenotype and AlgTube-VSMCs are closer to a contractile phenotype. AlgTube-VSMCs had enhanced expression of extracellular matrix (ECM) genes (*FN*, *COL4A6*, and *MMP9*) (Figure 5D), growth factors (*VEGFA* and *VEGFC*) (Figure 5E), and other genes related to angiogenesis (*PECAM1*, *ANGPT2*, *NOTCH4*, and *DLL4*) compared with 2D-VSMCs (Figure 5F). Using *Ki-67* immunostaining and flow cytometry analysis, we found more cells were proliferating in 2D-VSMCs (Figures 5G and 5H). These analyses well supported the RNA-seq data.

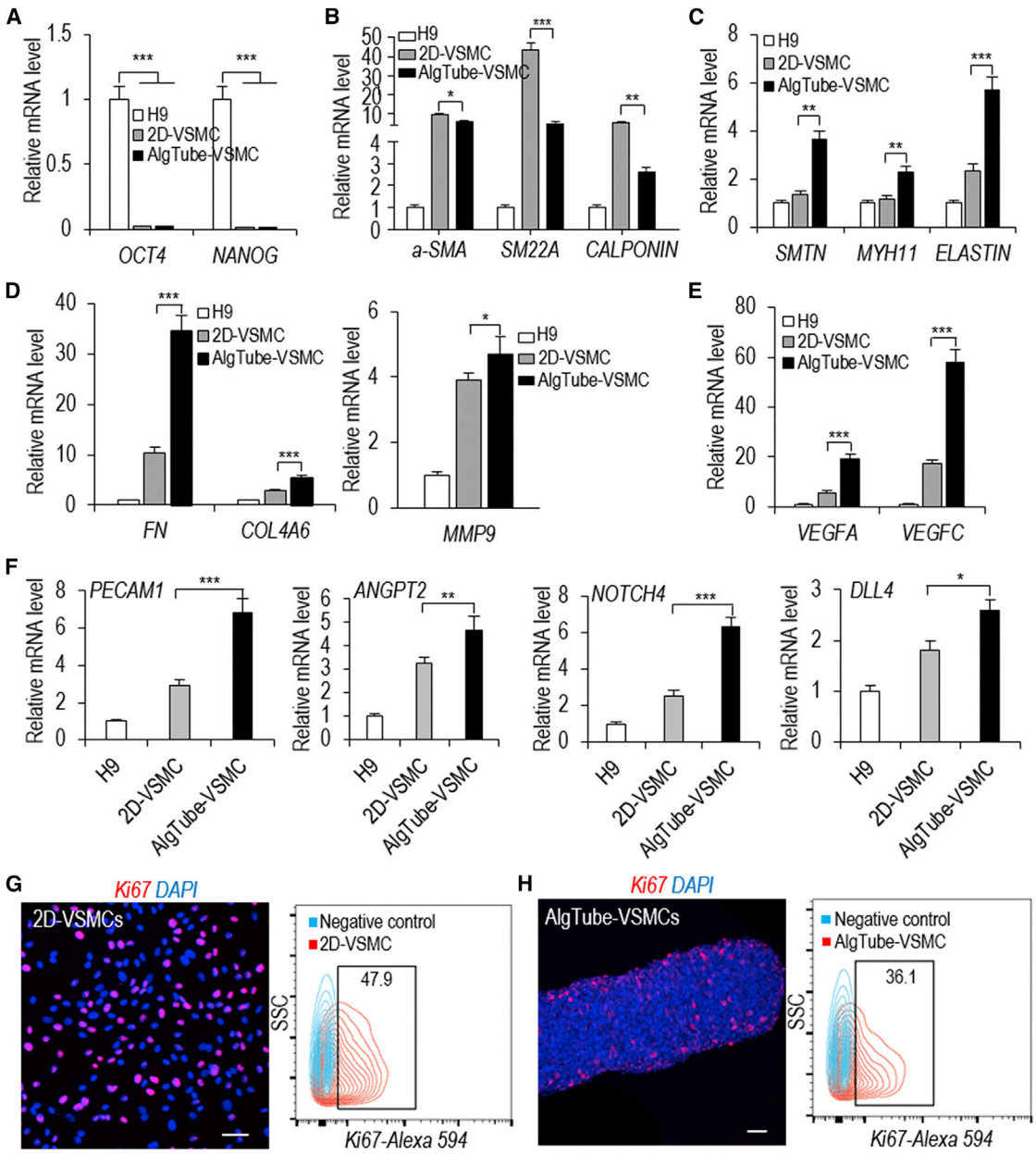

Figure 5. Gene Expression and Cell Proliferation Comparison of 2D-VSMCs and AlgTube-VSMCs

(A–F) qRT-PCR analyses of 2D-VSMCs, AlgTube-VSMCs, and H9 hESCs for (A) pluripotency markers *OCT4* and *NANOG*, (B) synthetic VSMC markers *α-SMA*, *SM22A*, and *CALPONIN*, (C) contractile VSMC markers *SMTN*, *MYH11*, and *ELASTIN*, (D) ECM genes *FN*, *COL4A*, and *MMP9*, (E) growth factors *VEGFA* and *VEGFC*, and (F) other genes related to angiogenesis, *PECAM1*, *ANGPT2*, *NOTCH4*, and *DLL4*. Data are represented as mean ± SD (n = 3). *p < 0.05, **p < 0.01, ***p < 0.001.

(G and H) Immunostaining and flow cytometry of *Ki67* showed that (G) 2D-VSMCs had more proliferating cells than (H) AlgTube-VSMCs. Scale bar, 50 μm.

Scalable Manufacturing of hPSC-VSMCs in a Bioreactor

The above studies were done using a small volume (e.g., <100 μL) of AlgTubes suspended in a six-well plate. We asked if AlgTubes could be suspended in a scalable bioreactor (Li et al., 2018a) for making hPSC-VSMCs at various scales (Figures 6A and 6B). Cells were expanded for 5 days and differentiated for 5 days in the bioreactor (Figure 6C). On day 10, hydrogel tubes were dissolved with EDTA and cells were harvested. Phase image and live/dead cell

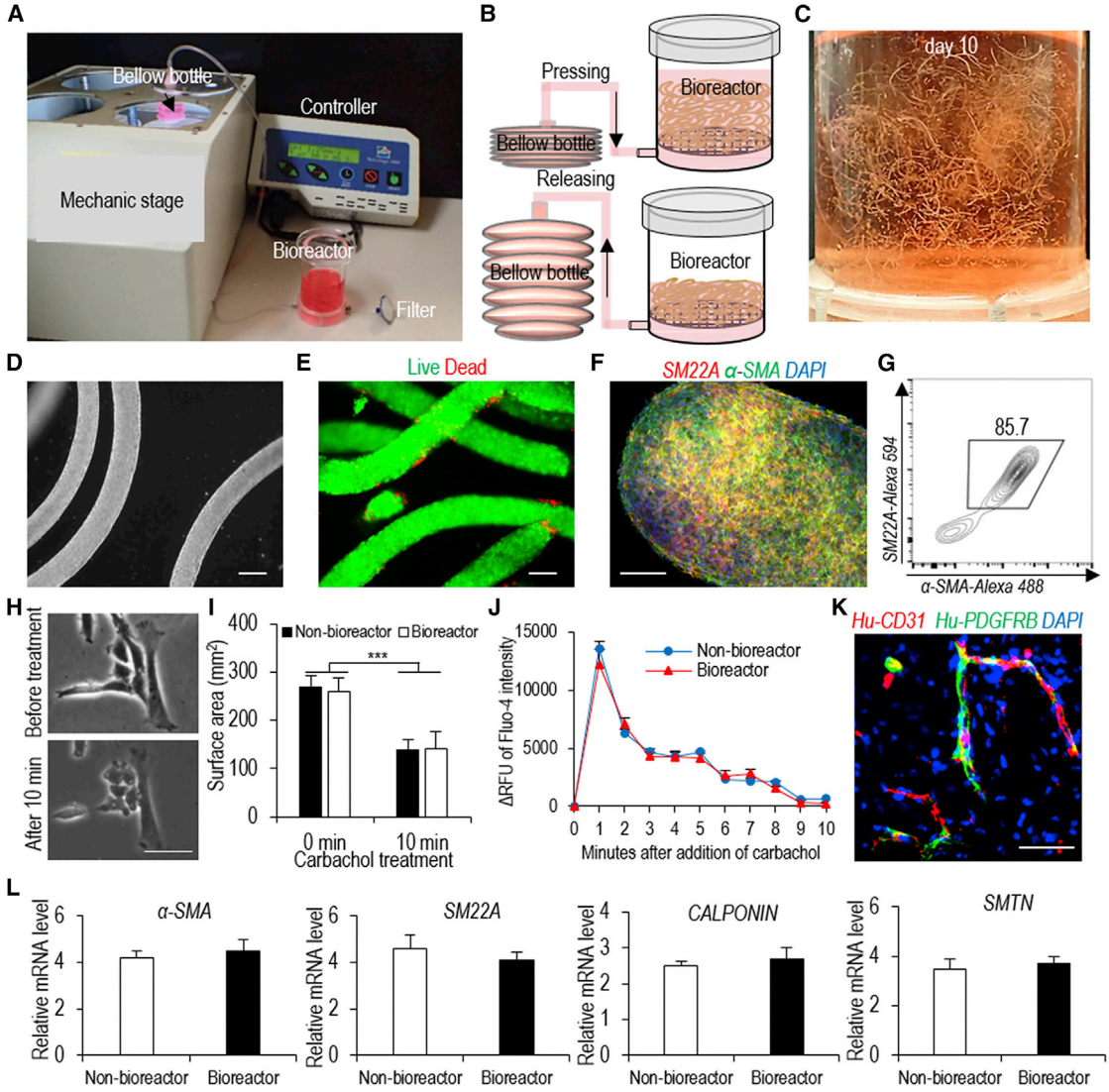

Figure 6. Making hPSC-VSMCs in a Bioreactor

(A) The bioreactor.

(B) Illustration of medium exchange.

(C) Day 10 cells in the bioreactor.

(D–G) (D) Phase, (E) live/dead cell staining, (F) immunostaining, and (G) flow cytometry analysis of day 10 cells from the bioreactor. Scale bars, 200, 50, and 20 μm, respectively.

(H and I) (H) Phase and (I) surface area of AlgTube-VSMCs made using the bioreactor in response to carbachol treatment. Scale bar, 50 μm. Data are represented as mean ± SD (n = 3). ***p < 0.001.

(J) The relative fluorescence units (ΔRFU) of Fluo-4-loaded VSMCs made with the bioreactor over 10 min after adding carbachol. Data are represented as mean ± SD (n = 3).

(K) When VSMCs made with the bioreactor and HUVECs were co-transplanted subcutaneously, they formed nice vascular structures. Scale bar, 50 μm.

(L) qRT-PCR analysis showed that AlgTube-VSMCs made using the bioreactor had similar expression levels of VSMC markers compared with AlgTube-VSMCs made using tissue culture plates (non-bioreactor). Data are represented as mean ± SD (n = 3).

staining showed that the majority of cells were live (Figures 6D and 6E). Flow cytometer analysis and immunostaining showed that 85.7% of the produced cells were VSMCs (Figures 6F and 6G). VSMCs produced in the bioreactor (bioreactor-VSMCs) contracted in response to carbachol treatment *in vitro* (Figures 6H and 6I). Calcium imaging

revealed that carbachol induced similar levels of intracellular calcium between bioreactor-VSMCs and non-bioreactor-VSMCs (i.e., AlgTube-VSMCs made using tissue culture plates) (Figure 6J). A transplantation study showed that bioreactor-VSMCs contributed to blood vessel formation *in vivo* (Figure 6K). Quantitative RT-PCR analysis showed that bioreactor-VSMCs had similar expression levels of VSMC markers compared with non-bioreactor-VSMCs (Figure 6L). We also showed that bioreactor-VSMCs could be cultured for multiple passages without losing their markers using the conventional 2D cultures (Figures S5F and S5G). These results show that AlgTubes are appropriate for preparing hPSC-VSMCs in a bioreactor. This prototype bioreactor can be scaled up for large-scale production in the future.

DISCUSSION

Generating enough hPSCs and their derivatives continues to be challenging. At present, hPSC-VSMCs are primarily made in 2D cultures (Patsch et al., 2015), which utilize growth conditions that are considerably different from the *in vivo* 3D microenvironment where cells reside (Chen et al., 2014b, 2014a; Kraehenbuehl et al., 2011; Thomson et al., 1998; Wong et al., 2010). Also, 2D culturing is not conducive to preparing large-scale cultures because it is labor, time, space, and reagent consuming (Kropp et al., 2017). Three-dimensional suspension culturing has successfully been shown to be an attractive method to scale up the production of hPSCs and their derivatives (Fridley et al., 2012; Kinney et al., 2011; Kropp et al., 2017). However, suspension growth of hPSCs continues to suffer from severe cellular agglomeration (Fridley et al., 2012; Kinney et al., 2011; Kropp et al., 2017). Applying agitation (stirring or shaking) to the culture can reduce agglomeration and recover mass transport (Fridley et al., 2012; Kinney et al., 2011; Kropp et al., 2017). However, agitation generates critical shear stress near the bioreactor wall and impeller tip that induces a large amount of cell death, leading to low cell expansion and yield (Fridley et al., 2012; Ismadi et al., 2014; Jenkins and Farid, 2015; Kinney et al., 2011; Kropp et al., 2017; Lei et al., 2014; Lei and Schaffer, 2013; Serra et al., 2012; Steiner et al., 2010). Agitation also generates complicated hydrodynamic conditions (e.g., the medium flow direction, velocity, shear force, and chemical environment) that vary spatially and temporally, and can be affected by a number of variables, including the design of the bioreactor (e.g., impeller geometry, size and position, vessel geometry and size, and positions of probes for pH, temperature, oxygen), the viscosity of the medium, and also the rate of agitation (Ismadi et al., 2014; Kropp et al., 2017). The hydrodynamic conditions are not very well understood yet, which makes them difficult to control (Fridley et al., 2012; Ismadi et al., 2014; Kinney et al., 2011; Kropp et al., 2017). This lack of understanding and technological issues causes considerable variability between culture batches, leading to further difficulty in scaling up culture size. For example, in recent 3D culture studies to generate cardiomyocytes from hPSCs, the cellular yield varied dramatically (from 40 million to 125 million cells) and the cellular purity varied from 28% to 88% in six different batches (100 mL culture volume) (Chen et al., 2015; Jara-avaca et al., 2014). When adjusting the culture volume from ~100 mL to ~1000 mL, both the efficiency of differentiation and the final product yield were altered significantly, which led to the need for reoptimization (Chen et al., 2015; Jara-avaca et al., 2014). This demonstrates the difficulty in scaling up further (e.g., hundreds of liters), due to the cost of optimizing multiple factors in a large volume. To date, <10 L of hPSC culture is the highest volume successfully produced (Kempf et al., 2016; Kropp et al., 2017). As a result, hydrodynamic conditions, and the associated critical stresses in combination with the uncontrolled cell aggregation, make it very challenging to utilize a 3D suspension culture system to generate hPSCs and their derivatives at large scales.

The alginate hydrogel tubes could eliminate both the cell agglomeration and the hydrodynamic stresses and their related adverse effects (Figures 1A–1C). Consequently, the culture efficiency (e.g., cell viability and yield) and consistency are significantly improved (Figures 1G and 1H). The volumetric yield reached 5.0×10^8 cells/mL of microspace, which is 250 times the current 3D suspension culturing. This high yield has enormous impact on large-scale cell production (Li et al., 2018a). Our calculations show that the cells would need to undergo passaging 10 times, ~32,753 L total bioreactor volume, and 45 days to produce $\sim 1.1 \times 10^{13}$ hPSC-VSMCs using 1.0×10^8 hPSCs as starting material. This production is technically and economically not feasible. Using AlgTubes, the same cells can be made using merely 320 L of hydrogel tubes, one passage, and 21 days. The reduction in culture volume, time, and passaging makes the production technically and economically feasible.

Our research showed that the differentiation efficiencies in 2D and AlgTubes were similar (Figures 2 and S2), indicating that the differentiation protocol developed by Patsch (Patsch et al., 2015) using 2D cultures can be used for 3D culture. Phenotype assays and genome-wide gene expression analysis showed that AlgTube-VSMCs and 2D-VSMCs were similar overall. Both of them had typical VSMC phenotypes (Figure 3). Transplantation studies showed that AlgTube-VSMCs and 2D-VSMCs contributed to blood vessel formation similarly *in vivo* (Figures 3I and 3J). However, they do have some differences in global

gene expression. AlgTube-VSMCs had higher expression of genes related to vasculature development, angiogenesis, and cell migration (Figure 4D). This agrees with recent research on organoids, which shows that 3D microenvironments promote tissue formation (Hattori, 2014; Jo et al., 2016; Takahashi et al., 2018). 2D-VSMCs are closer to the synthetic phenotype. For instance, they had higher proliferation (Figure 5G) and higher expression of the synthetic VSMC genes (Figure 5B). Two-dimensional culturing on a stiff substrate induces cell proliferation, which is a frequently observed phenomenon when culturing primary human cells (Chamley et al., 1977; Timraz et al., 2015; Wazen et al., 2013). Both AlgTube-VSMCs and 2D-VSMCs had some differences in global gene expression from the primary HASMCs. If and how the differences in global gene expression between the three types of VSMCs affect their phenotypes and functions should be made clear in the future using more sensitive assays and disease models.

Conclusion

In summary, we have developed a scalable method for manufacturing VSMCs from hPSCs with high viability, high purity (>80%), and high yield (~5.0×10^8 cells/mL of microspace). The method will make VSMCs broadly available and affordable for various applications.

EXPERIMENTAL PROCEDURES

RNA Sequencing and Data Analysis

Total RNA of day 6 VSMCs from 2D culture and day 10 VSMCs from AlgTubes (note: both VSMCs were differentiated for 5 days) was prepared with an RNeasy mini kit (Cat. No. 74,104; QIAGEN) according to the manufacturer's instructions. Prior to RNA-seq, magnetic beads coated with anti-CD144 antibodies were added to remove CD144+ hPSC-ECs with a magnetic cell separator. VSMCs reached 95% purity after purification. Libraries were prepared with a TruSeq Stranded mRNA Library Prep Kit and sequenced with Illumina NextSeq 500. Twenty million 75 bp paired-end reads were generated for each sample. The thresholds for differential expression were set at fold-change > 2 and adjusted $p < 0.001$ for the null hypothesis. Methods for the data processing, generation of heatmaps, PCA, and differential gene expression analysis have been described in our previous publication (Li et al., 2018a).

Statistical Analysis

The data are presented as the mean ± SD from three independent experiments. We used an unpaired t test to compare two groups and one-way ANOVA to compare more than two groups. A sample size of 3 was selected so that at a significance level of 0.05 there was at least a 95% chance of detecting a 2 SD difference in outcome between the groups. All data were processed using GraphPad Prism 7 (GraphPad Software, La Jolla, CA).

ACCESSION NUMBERS

The final processed data and raw fastq files were submitted to Gene Expression Omnibus (GEO) with the accession numbers GEO: GSE99776 and GSE109683. All other data supporting the findings of this study are available within the paper and its Supplemental Information.

SUPPLEMENTAL INFORMATION

Supplemental Information includes Supplemental Experimental Procedures, seven figures, and three tables and can be found with this article online at https://doi.org/10.1016/j.stemcr.2018.11.009.

AUTHOR CONTRIBUTIONS

Y.L. and H.L. conceived the idea, designed the experiments, and wrote the manuscript. L.A. made the device. H.L., X.Q., Q.L., and O.W. performed the experiments. H.L., X.Q., Q.D., K.L., and C.Z. analyzed the data. D.A. contributed to flow cytometry analysis. Z.W. and L.G. revised the manuscript.

ACKNOWLEDGMENTS

This work was partially funded by the UNL-UNMC Science Engineering and Medicine (SEM) initiative grant. Confocal microscope imaging was done in the Morrison Microscopy Core Research Facility at the University of Nebraska, Lincoln. Dr. You Zhou and Dr. Christian Elowsky assisted in the confocal imaging. Flow cytometry was done in the Morrison Center, the Flow Cytometry Service Center, University of Nebraska, Lincoln, with the assistance of Dirk Anderson. RNA sequencing was done at the UNMC deep sequencing core.

Received: August 6, 2018
Revised: November 12, 2018
Accepted: November 13, 2018
Published: December 6, 2018

REFERENCES

Alexander, M.R., and Owens, G.K. (2012). Epigenetic control of smooth muscle cell differentiation and phenotypic switching in vascular development and disease. Annu. Rev. Physiol. *74*, 13–40.

Ayoubi, S., Sheikh, S.P., and Eskildsen, T.V. (2017). Human induced pluripotent stem cell-derived vascular smooth muscle cells: differentiation and therapeutic potential. Cardiovasc. Res. *113*, 1282–1293.

Bajpai, V.K., Mistriotis, P., Loh, Y.-H., Daley, G.Q., and Andreadis, S.T. (2012). Functional vascular smooth muscle cells derived from human induced pluripotent stem cells via mesenchymal stem cell intermediates. Cardiovasc. Res. *96*, 391–400.

Bao, X., Lian, X., Dunn, K.K., Shi, M., Han, T., Qian, T., Bhute, V.J., Canfield, S.G., and Palecek, S.P. (2015). Chemically-defined albumin-free differentiation of human pluripotent stem cells to endothelial progenitor cells. Stem Cell Res. *15*, 122–129.

Bernardo, A.S., Faial, T., Gardner, L., Niakan, K.K., Ortmann, D., Senner, C.E., Callery, E.M., Trotter, M.W., Hemberger, M., Smith, J.C., et al. (2011). BRACHYURY and CDX2 mediate BMP-induced

differentiation of human and mouse pluripotent stem cells into embryonic and extraembryonic lineages. Cell Stem Cell *9*, 144–155.

Biel, N.M., Santostefano, K.E., DiVita, B.B., El Rouby, N., Carrasquilla, S.D., Simmons, C., Nakanishi, M., Cooper-DeHoff, R.M., Johnson, J.A., and Terada, N. (2015). Vascular smooth muscle cells from hypertensive patient-derived induced pluripotent stem cells to advance hypertension pharmacogenomics. Stem Cells Transl. Med. *4*, 1380–1390.

Carmeliet, P. (2000). Mechanisms of angiogenesis and arteriogenesis. Nat. Med. *6*, 389–395.

Chamley, J.H., Campbell, G.R., McConnell, J.D., and Gröschel-Stewart, U. (1977). Comparison of vascular smooth muscle cells from adult human, monkey and rabbit in primary culture and in subculture. Cell Tissue Res. *177*, 503–522.

Chen, G., Gulbranson, D.R., Hou, Z., Bolin, J.M., Ruotti, V., Probasco, M.D., Smuga-Otto, K., Howden, S.E., Diol, N.R., Propson, N.E., et al. (2011). Chemically defined conditions for human iPSC derivation and culture. Nat. Methods *8*, 424–429.

Chen, K.G., Mallon, B.S., Johnson, K.R., Hamilton, R.S., Mckay, R.D.G., and Robey, P.G. (2014a). Developmental insights from early mammalian embryos and core signaling pathways that influence human pluripotent cell growth and differentiation. Stem Cell Res. *12*, 610–621.

Chen, K.G., Mallon, B.S., McKay, R.D.G., and Robey, P.G. (2014b). Human pluripotent stem cell culture: considerations for maintenance, expansion, and therapeutics. Cell Stem Cell *14*, 13–26.

Chen, V.C., Ye, J., Shukla, P., Hua, G., Chen, D., Lin, Z., Liu, J., Chai, J., Gold, J., Wu, J., et al. (2015). Development of a scalable suspension culture for cardiac differentiation from human pluripotent stem cells. Stem Cell Res. *15*, 365–375.

Cheung, C., Bernardo, A.S., Trotter, M.W.B., Pedersen, R.A., and Sinha, S. (2012). Generation of human vascular smooth muscle subtypes provides insight into embryological origin–dependent disease susceptibility. Nat. Biotechnol. *30*, 165–173.

Cheung, C., Bernardo, A.S., Pedersen, R.A., and Sinha, S. (2014). Directed differentiation of embryonic origin-specific vascular smooth muscle subtypes from human pluripotent stem cells. Nat. Protoc. *9*, 929–938.

Emilio, R., Antonio, G.-M., Eugenia, P., Santiago, R., Enrique, R., Fernando, R., Ana, M.B., Cornelis, van B., Elena, O., and Teresa, T. (2006). Human vascular smooth muscle cells from diabetic patients are resistant to induced apoptosis due to high Bcl-2 expression. Diabetes *55*, 1243–1251.

Eoh, J.H., Shen, N., Burke, J.A., Hinderer, S., Xia, Z., Schenke-Layland, K., and Gerecht, S. (2017). Enhanced elastin synthesis and maturation in human vascular smooth muscle tissue derived from induced-pluripotent stem cells. Acta Biomater. *52*, 49–59.

Ferreira, L.S., Gerecht, S., Shieh, H.F., Watson, N., Rupnick, M.A., Dallabrida, S.M., Vunjak-novakovic, G., and Langer, R. (2007). Vascular progenitor cells isolated from human embryonic stem cells give rise to endothelial and smooth muscle like cells and form vascular networks in vivo. Circ. Res. *101*, 286–294.

Fridley, K.M., Kinney, M.A., and Mcdevitt, T.C. (2012). Hydrodynamic modulation of pluripotent stem cells. Stem Cell Res. Ther. *3*, 45.

Ge, X., Ren, Y., Bartulos, O., Lee, M.Y., Yue, Z., Kim, K.Y., Li, W., Amos, P.J., Bozkulak, E.C., Iyer, A., et al. (2012). Modeling supravalvular aortic stenosis syndrome with human induced pluripotent stem cells. Circulation *126*, 1695–1704.

Gerecht, S., Ferreira, L.S., and Langer, R. (2010). Vascular differentiation of human embryonic stem cells in bioactive hydrogel-based scaffolds. Methods Mol. Biol. *584*, 333–354.

Granata, A., Serrano, F., Bernard, W.G., McNamara, M., Low, L., Sastry, P., and Sinha, S. (2017). An iPSC-derived vascular model of Marfan syndrome identifies key mediators of smooth muscle cell death. Nat. Genet. *49*, 97–109.

Hattan, N., Warltier, D., Gu, W., Kolz, C., Chilian, W.M., and Weihrauch, D. (2004). Autologous vascular smooth muscle cell-based myocardial gene therapy to induce coronary collateral growth. Am. J. Physiol. Circ. Physiol. *287*, H488–H493.

Hattori, N. (2014). Cerebral organoids model human brain development and microcephaly. Mov. Disord. *29*, 185.

Hibino, N., Duncan, D.R., Nalbandian, A., Yi, T., Qyang, Y., Shinoka, T., and Breuer, C.K. (2012). Evaluation of the use of an induced pluripotent stem cell sheet for the construction of tissue-engineered vascular grafts. J. Thorac. Cardiovasc. Surg. *143*, 696–703.

Hong, X., Margariti, A., Le Bras, A., Jacquet, L., Kong, W., Hu, Y., and Xu, Q. (2017). Transdifferentiated human vascular smooth muscle cells are a new potential cell source for endothelial regeneration. Sci. Rep. *7*, 5590.

Ismadi, M., Gupta, P., Fouras, A., Verma, P., and Jadhav, S. (2014). Flow characterization of a spinner flask for induced pluripotent stem cell culture application. PLoS One *9*, e106493.

Iyer, D., Gambardella, L., Bernard, W.G., Serrano, F., Mascetti, V.L., Pedersen, R.A., Sinha, S., and Talasila, A. (2016). Robust derivation of epicardium and its differentiated smooth muscle cell progeny from human pluripotent stem cells. Development *143*, 904.

Jara-avaca, M., Kempf, H., Olmer, R., Kropp, C., Ru, M., Robles-diaz, D., Franke, A., Elliott, D.A., Wojciechowski, D., Fischer, M., et al. (2014). Controlling expansion and cardiomyogenic differentiation of human pluripotent stem cells in scalable suspension culture. Stem Cell Reports *3*, 1132–1146.

Jenkins, M.J., and Farid, S.S. (2015). Human pluripotent stem cell-derived products: advances towards robust, scalable and cost-effective manufacturing strategies. Biotechnol. J. *10*, 83–95.

Ji, H., Kim, H.S., Kim, H.-W., and Leong, K.W. (2017). Application of induced pluripotent stem cells to model smooth muscle cell function in vascular diseases. Curr. Opin. Biomed. Eng. *1*, 38–44.

Jo, J., Xiao, Y., Sun, A.X., Cukuroglu, E., Tran, H.D., Göke, J., Tan, Z.Y., Saw, T.Y., Tan, C.P., Lokman, H., et al. (2016). Midbrain-like organoids from human pluripotent stem cells contain functional dopaminergic and neuromelanin-producing neurons. Cell Stem Cell *19*, 248–257.

Karamariti, E., Margariti, A., Winkler, B., Wang, X., Hong, X., Baban, D., Ragoussis, J., Huang, Y., Han, J.D.J., Wong, M.M., et al. (2013). Smooth muscle cells differentiated from reprogrammed embryonic lung fibroblasts through dkk3 signaling are potent for tissue engineering of vascular grafts. Circ. Res. *112*, 1433–1443.

Kempf, H., Andree, B., and Zweigerdt, R. (2016). Large-scale production of human pluripotent stem cell derived cardiomyocytes. Adv. Drug Deliv. Rev. *96*, 18–30.

Kinnear, C., Chang, W.Y., Khattak, S., Hinek, A., Thompson, T., Rodrigues, D., de, C., Kennedy, K., Mahmut, N., Pasceri, P., et al. (2013a). Modeling human protein aggregation cardiomyopathy using murine induced pluripotent stem cells. Stem Cell Transl. Med. *2*, 161–166.

Kinnear, C., Chang, W., Khattak, S., Hinek, A., Thompson, T., de Carvalho Rodrigues, D., Kennedy, K., Mahmut, N., Pasceri, P., Stanford, W., et al. (2013b). Modeling and rescue of the vascular phenotype of Williams-Beuren syndrome in patient induced pluripotent stem cells. Stem Cells Transl. Med. *2*, 2–15.

Kinney, M.A., Sargent, C.Y., and Mcdevitt, T.C. (2011). The multiparametric effects of hydrodynamic environments on stem cell culture. Tissue Eng. Part B Rev. *17*, 249–262.

Kraehenbuehl, T.P., Langer, R., and Ferreira, L.S. (2011). Three-dimensional biomaterials for the study of human pluripotent stem cells. Nat. Methods *8*, 731–736.

Kropp, C., Massai, D., and Zweigerdt, R. (2017). Progress and challenges in large-scale expansion of human pluripotent stem cells. Process. Biochem. *59*, 244–254.

Lacolley, P., Regnault, V., Nicoletti, A., Li, Z., and Michel, J.B. (2012). The vascular smooth muscle cell in arterial pathology: a cell that can take on multiple roles. Cardiovasc. Res. *95*, 194–204.

Lalit, P.A., Hei, D.J., Raval, A.N., and Kamp, T.J. (2014). Induced pluripotent stem cells for post -myocardial infarction repair. Circ. Res. *114*, 1328–1345.

Lee, T.-H., Song, S.-H., Kim, K.L., Yi, J.-Y., Shin, G.-H., Kim, J.Y., Kim, J., Han, Y.-M., Lee, S.H., Lee, S.-H., et al. (2010). Functional recapitulation of smooth muscle cells via induced pluripotent stem cells from human aortic smooth muscle cells. Circ. Res. *106*, 120–128.

Lei, Y., and Schaffer, D.V. (2013). A fully defined and scalable 3D culture system for human pluripotent stem cell expansion and differentiation. Proc. Natl. Acad. Sci. U S A *110*, E5039–E5048.

Lei, Y., Jeong, D., Xiao, J., and Schaffer, D.V. (2014). Developing defined and scalable 3D culture systems for culturing human pluripotent stem cells at high densities. Cell. Mol. Bioeng. *7*, 172–183.

Levenberg, S. (2005). Engineering blood vessels from stem cells: recent advances and applications. Curr. Opin. Biotechnol. *16*, 516–523.

Levenberg, S., Zoldan, J., Basevitch, Y., and Langer, R. (2007). Endothelial potential of human embryonic stem cells. Blood *110*, 806–814.

Li, Q., Lin, H., Du, Q., Liu, K., Wang, O., Evans, C., Christian, H., Zhang, C., and Lei, Y. (2018a). Scalable and physiologically relevant microenvironments for human pluripotent stem cell expansion and differentiation. Biofabrication *10*, 025006.

Li, Q., Lin, H., Rauch, J., Deleyrolle, L.P., Reynolds, B.A., Viljoen, H.J., Zhang, C., Zhang, C., Gu, L., Van Wyk, E., et al. (2018b). Scalable culturing of primary human glioblastoma tumor-initiating cells with a cell-friendly culture system. Sci. Rep. *8*, 3531.

Li, R.-K., Jia, Z.-Q., Weisel, R.D., Merante, F., and Mickle, D.A.G. (1999). Smooth muscle cell transplantation into myocardial scar tissue improves heart function. J. Mol. Cell. Cardiol. *31*, 513–522.

Lian, X., Bao, X., Al-Ahmad, A., Liu, J., Wu, Y., Dong, W., Dunn, K.K., Shusta, E.V., and Palecek, S.P. (2014). Efficient differentiation of human pluripotent stem cells to endothelial progenitors via small-molecule activation of WNT signaling. Stem Cell Reports *3*, 804–816.

Lin, B., Kim, J., Li, Y., Pan, H., Carvajal-Vergara, X., Salama, G., Cheng, T., Li, Y., Lo, C.W., and Yang, L. (2012). High-purity enrichment of functional cardiovascular cells from human iPS cells. Cardiovasc. Res. *95*, 327–335.

Lin, H., Du, Q., Li, Q., Wang, O., Wang, Z., Liu, K., Elowsky, C., Zhang, C., and Lei, Y. (2018a). A hydrogel-based bioprocess for scalable manufacturing of human pluripotent stem cells-derived neural stem cells. ACS Appl. Mater. Interfaces *10*, 29238–29250.

Lin, H., Li, Q., Wang, O., Rauch, J., Harm, B., Viljoen, H.J., Zhang, C., Van Wyk, E., Zhang, C., and Lei, Y. (2018b). Automated expansion of primary human T cells in scalable and cell-friendly hydrogel microtubes for adoptive immunotherapy. Adv. Healthc. Mater. *7*, e1701297.

Liu, G.H., Barkho, B.Z., Ruiz, S., Diep, D., Qu, J., Yang, S.L., Panopoulos, A.D., Suzuki, K., Kurian, L., Walsh, C., et al. (2011). Recapitulation of premature ageing with iPSCs from Hutchinson-Gilford progeria syndrome. Nature *472*, 221–227.

Louis, S.F., and Zahradka, P. (2010). Vascular smooth muscle cell motility: from migration to invasion. Exp. Clin. Cardiol. *15*, e75–e85.

Mark, W.M., and Christine, L.M. (2012). Smooth muscle diversity from human pluripotent cells. Nat. Biotechnol. *30*, 152–154.

Matsubayashi, K., Fedak, P., Mickle, D., Weisel, R., Ozawa, T., and Li, R. (2003). Improved left ventricular aneurysm repair with bioengineered vascular smooth muscle grafts. Circulation *108*, II219–II225.

Melanie, M., Erica, K.A., Smruti, M.P., Michael, T.L., John, P.C., Bertha, C., et al. (2014). Concurrent generation of functional smooth muscle and endothelial cells via a vascular progenitor. Stem Cells Transl. Med. *3*, 91–97.

Okita, K., Matsumura, Y., Sato, Y., Okada, A., Morizane, A., Okamoto, S., Hong, H., Nakagawa, M., Tanabe, K., Tezuka, K., et al. (2011). A more efficient method to generate integration-free human iPS cells. Nat. Methods *8*, 409–412.

Owens, G.K., Kumar, M.S., and Wamhoff, B.R. (2004). Molecular regulation of vascular smooth muscle cell differentiation in development and disease. Physiol. Rev. *84*, 767–801.

Pan, X., Wang, B., Yuan, T., Zhang, M., Kent, K.C., and Guo, L.W. (2018). Analysis of combined transcriptomes identifies gene modules that differentially respond to pathogenic stimulation of vascular smooth muscle and endothelial cells. Sci. Rep. *8*, 395.

Park, I.H., Zhao, R., West, J.A., Yabuuchi, A., Huo, H., Ince, T.A., Lerou, P.H., Lensch, M.W., and Daley, G.Q. (2008). Reprogramming of human somatic cells to pluripotency with defined factors. Nature *451*, 141–146.

Park, S., Koh, Y.J., Jeon, J., Cho, Y., Jang, M., Kang, Y., Kim, M., Choi, C., Cho, Y.S., Chung, H., et al. (2010). Efficient differentiation of

human pluripotent stem cells into functional CD34+ progenitor cells by combined modulation of the MEK/ERK and BMP4 signaling pathways. Blood *116*, 5762–5772.

Patsch, C., Challet-Meylan, L., Thoma, E.C., Urich, E., Heckel, T., O'Sullivan, J.F., Grainger, S.J., Kapp, F.G., Sun, L., Christensen, K., et al. (2015). Generation of vascular endothelial and smooth muscle cells from human pluripotent stem cells. Nat. Cell Biol. *17*, 994–1003.

Pei, D., Xu, J., Zhuang, Q., Tse, H.-F., and Esteban, M.A. (2010). Induced pluripotent stem cell technology in regenerative medicine and biology. Adv. Biochem. Eng. Biotechnol. *123*, 127–141.

Poh, M., Boyer, M., Solan, A., Dahl, S.L., Pedrotty, D., Banik, S.S., McKee, J.A., Klinger, R.Y., Counter, C.M., and Niklason, L.E. (2005). Blood vessels engineered from human cells. Lancet *365*, 2122–2124.

Porter, K.E., and Riches, K. (2013). The vascular smooth muscle cell: a therapeutic target in Type 2 diabetes? Clin. Sci. (Lond.) *125*, 167–182.

Raphel, L., Talasila, A., Cheung, C., and Sinha, S. (2012). Myocardin overexpression is sufficient for promoting the development of a mature smooth muscle cell-like phenotype from human embryonic stem cells. PLoS One *7*, e44052.

Serra, M., Brito, C., Correia, C., and Alves, P.M. (2012). Process engineering of human pluripotent stem cells for clinical application. Trends Biotechnol. *30*, 350–358.

Sinha, S., Hoofnagle, M.H., Kingston, P.A., Mccanna, M.E., and Owens, G.K. (2004). Transforming growth factor-beta 1 signaling contributes to development of smooth muscle cells from embryonic stem cells. Am. J. Physiol. Cell Physiol. *287*, C1560–C1568.

Staudacher, D.L., Preis, M., Lewis, B.S., Grossman, P.M., and Flugelman, M.Y. (2006). Cellular and molecular therapeutic modalities for arterial obstructive syndromes. Pharmacol. Ther. *109*, 263–273.

Steiner, D., Khaner, H., Cohen, M., Even-Ram, S., Gil, Y., Itsykson, P., Turetsky, T., Idelson, M., Aizenman, E., Ram, R., et al. (2010). Derivation, propagation and controlled differentiation of human embryonic stem cells in suspension. Nat. Biotechnol. *28*, 361–364.

Takahashi, K., Tanabe, K., Ohnuki, M., Narita, M., Ichisaka, T., Tomoda, K., and Yamanaka, S. (2007). Induction of pluripotent stem cells from adult human fibroblasts by defined factors. Cell *131*, 861–872.

Takahashi, Y., Sato, S., Kurashima, Y., Yamamoto, T., Kurokawa, S., Yuki, Y., Takemura, N., Uematsu, S., Lai, C., Otsu, M., et al. (2018). A refined culture system for human induced pluripotent stem cell-derived intestinal epithelial organoids. Stem Cell Reports *10*, 314–328.

Taura, D., Sone, M., Homma, K., Oyamada, N., Takahashi, K., Tamura, N., Yamanaka, S., and Nakao, K. (2009). Induction and isolation of vascular cells from human induced pluripotent stem cells—brief report. Arterioscler. Thromb. Vasc. Biol. *29*, 1100–1103.

Thomson, J.A., Itskovitz-eldor, J., Shapiro, S.S., Waknitz, M.A., Swiergiel, J.J., Marshall, V.S., and Jones, J.M. (1998). Embryonic stem cell lines derived from human blastocysts. Science *282*, 1145–1147.

Timraz, S.B.H., Rezgui, R., Boularaoui, S.M., and Teo, J.C.M. (2015). Stiffness of extracellular matrix components modulates the phenotype of human smooth muscle cells in vitro and allows for the control of properties of engineered tissues. Procedia Eng. *110*, 29–36.

Vo, E., Hanjaya-Putra, D., Zha, Y., Kusuma, S., and Gerecht, S. (2010). Smooth-muscle-like cells derived from human embryonic stem cells support and augment cord-like structures in vitro. Stem Cell Rev. Rep. *6*, 237–247.

Wang, Y., Hu, J., Jiao, J., Liu, Z., Zhou, Z., Zhao, C., Chang, L.J., Chen, Y.E., Ma, P.X., and Yang, B. (2014). Engineering vascular tissue with functional smooth muscle cells derived from human iPS cells and nanofibrous scaffolds. Biomaterials *35*, 8960–8969.

Wang, Z., Wen, Y., Li, Y.H., Wei, Y., Green, M., Wani, P., Zhang, P., Pera, R.R., and Chen, B. (2016). Smooth muscle precursor cells derived from human pluripotent stem cells for treatment of stress urinary incontinence. Stem Cells Dev. *25*, 453–461.

Wanjare, M., Kuo, F., and Gerecht, S. (2013). Derivation and maturation of synthetic and contractile vascular smooth muscle cells from human pluripotent stem cells. Cardiovasc. Res. *97*, 321–330.

Wanjare, M., Agarwal, N., and Gerecht, S. (2015). Biomechanical strain induces elastin and collagen production in human pluripotent stem cell-derived vascular smooth muscle cells. Am. J. Physiol. Cell Physiol. *309*, C271–C281.

Wazen, R.M., Kuroda, S., Nishio, C., Sellin, K., Brunski, J.B., and Nanci, A. (2013). The effect of substrate modulus on the growth and function of matrix-embedded endothelial cells. Biomaterials *34*, 677–684.

Wong, C.C., Loewke, K.E., Bossert, N.L., Behr, B., De Jonge, C.J., Baer, T.M., and Pera, R.A.R. (2010). Non-invasive imaging of human embryos before embryonic genome activation predicts development to the blastocyst stage. Nat. Biotechnol. *28*, 1115–1121.

Wurm, F.M. (2004). Production of recombinant protein therapeutics in cultivated mammalian cells. Nat. Biotechnol. *22*, 1393–1398.

Yang, L., Geng, Z., Nickel, T., Johnson, C., Gao, L., Dutton, J., Hou, C., and Zhang, J. (2016). Differentiation of human induced-pluripotent stem cells into smooth-muscle cells: two novel protocols. PLoS One *11*, e0147155.

Ye, L., Chang, Y.H., Xiong, Q., Zhang, P., Zhang, L., Somasundaram, P., Lepley, M., Swingen, C., Su, L., Wendel, J.S., et al. (2014). Cardiac repair in a porcine model of acute myocardial infarction with human induced pluripotent stem cell-derived cardiovascular cells. Cell Stem Cell *15*, 750–761.

Yoo, C.H., Na, H.J., Lee, D.S., Heo, S.C., An, Y., Cha, J., Choi, C., Kim, J.H., Park, J.C., and Cho, Y.S. (2013). Endothelial progenitor cells from human dental pulp-derived iPS cells as a therapeutic target for ischemic vascular diseases. Biomaterials *34*, 8149–8160.

Yu, J., Vodyanik, M.A., Smuga-otto, K., Antosiewicz-bourget, J., Frane, J.L., Tian, S., Nie, J., Jonsdottir, G.A., Ruotti, V., Stewart, R., et al. (2007). Induced pluripotent stem cell lines derived from human somatic cells. Science *318*, 1917–1920.

Zhang, H., Xiong, Z.-M., and Cao, K. (2014). Mechanisms controlling the smooth muscle cell death in progeria via down-regulation of poly(ADP-ribose) polymerase 1. Proc. Natl. Acad. Sci. U S A *111*, E2261–E2270.

Zhang, J., Lian, Q., Zhu, G., Zhou, F., Sui, L., Tan, C., Mutalif, R.A., Navasankari, R., Zhang, Y., Tse, H.F., et al. (2011). A human iPSC model of Hutchinson Gilford Progeria reveals vascular smooth muscle and mesenchymal stem cell defects. Cell Stem Cell *8*, 31–45.

Stem Cell Reports, Volume *12*

Supplemental Information

Engineered Microenvironment for Manufacturing Human Pluripotent Stem Cell-Derived Vascular Smooth Muscle Cells

Haishuang Lin, Xuefeng Qiu, Qian Du, Qiang Li, Ou Wang, Leonard Akert, Zhanqi Wang, Dirk Anderson, Kan Liu, Linxia Gu, Chi Zhang, and Yuguo Lei

Supplemental Information

Engineered Microenvironment for Manufacturing Human Pluripotent Stem Cells Derived Vascular Smooth Muscle Cells

Haishuang Lin[1,10], Xuefeng Qiu[2,10], Qian Du[3], Qiang Li[1,4], Ou Wang[1,4], Leonard Akert[1], Zhanqi Wang[5], Dirk Anderson[6], Kan Liu[3], Linxia Gu[7], Chi Zhang[3] and Yuguo Lei[1,4,8,9*]

1: Department of Chemical and Biomolecular Engineering, University of Nebraska-Lincoln, Nebraska, USA

2: Department of cardiovascular surgery, Union Hospital, Tongji Medical College, Huazhong University of Science and Technology, Wuhan, China

3: Department of Biological Systems Engineering, University of Nebraska-Lincoln, Nebraska, USA

4: Biomedical Engineering Program, University of Nebraska-Lincoln, Nebraska, USA

5: Department of Vascular Surgery, Beijing Anzhen Hospital of Capital Medical University, Beijing Institute of Heart Lung and Blood Vessel Diseases, Beijing, China

6: Center for Biotechnology, University of Nebraska-Lincoln, Nebraska, USA

7: Department of Mechanical and Materials Engineering, University of Nebraska-Lincoln, Nebraska, USA

8: Mary and Dick Holland Regenerative Medicine Program, University of Nebraska Medical Center, Omaha, Nebraska, USA

9: Fred & Pamela Buffett Cancer Center, University of Nebraska Medical Center, Omaha, Nebraska, USA

10: These authors contribute equally to this work.

* Corresponding Author

Yuguo Lei

820 N 16th St

Lincoln, NE 68588

Email: ylei14@unl.edu

Phone: 402-472-5313

Fax: 402-472-6989

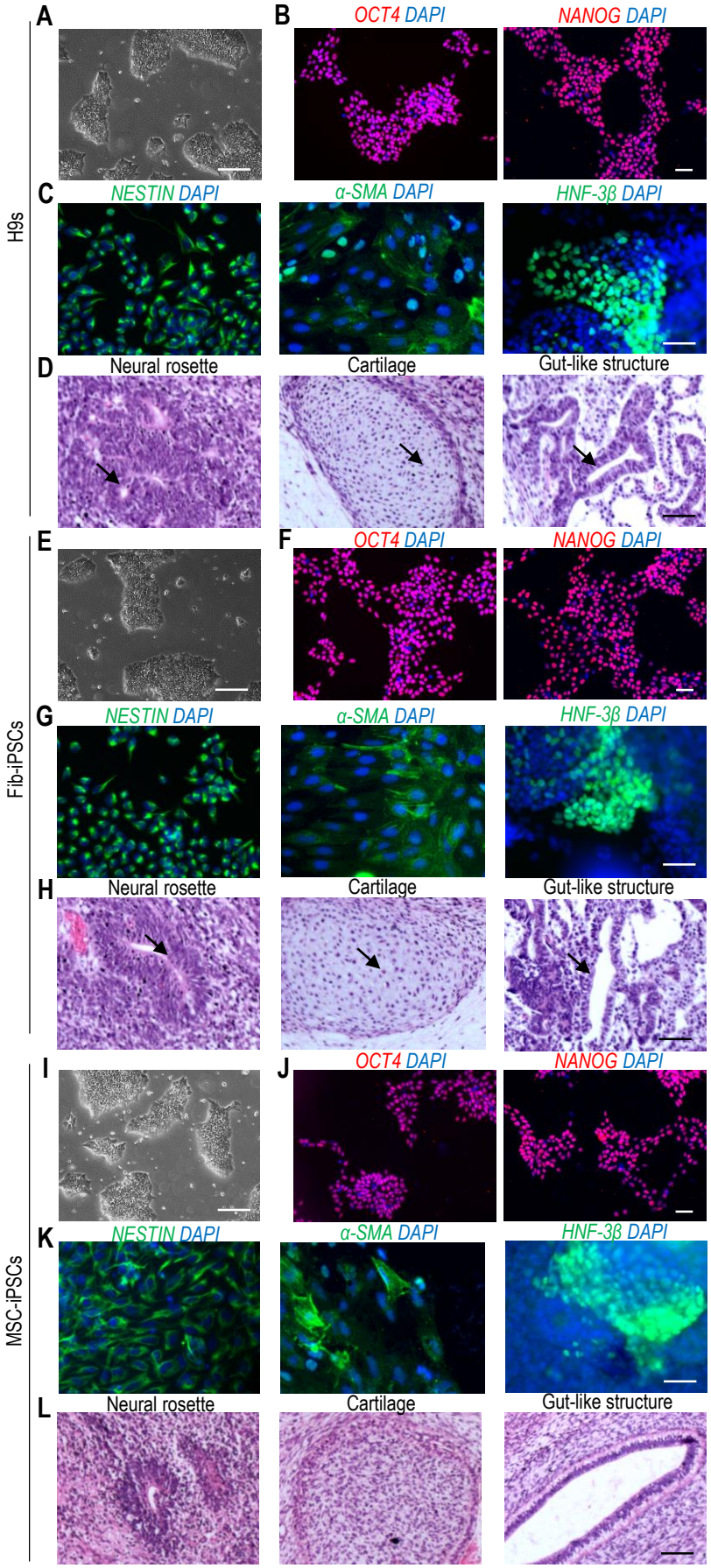

Figure S1. Starting hPSCs (H9s, Fib-iPSCs and MSC-iPSCs).
(**A, E, I**) Phase images. Scale bar, 200 μm.
(**B, F, J**) Majority of the cells expressed the pluripotency markers, *OCT4* and *NANOG*. Scale bar, 50 μm.
(**C, G, K**) They could be differentiated into all three germ layer cells such as *NESTIN*+ ectodermal, *α-SMA*+ mesodermal and *HNF-3β*+ endodermal cells in EB assay. Scale bar, 50 μm.
(**D, H, L**) They formed teratomas containing all three germ layer tissues (arrows) in SCID mice. Scale bar, 50 μm.

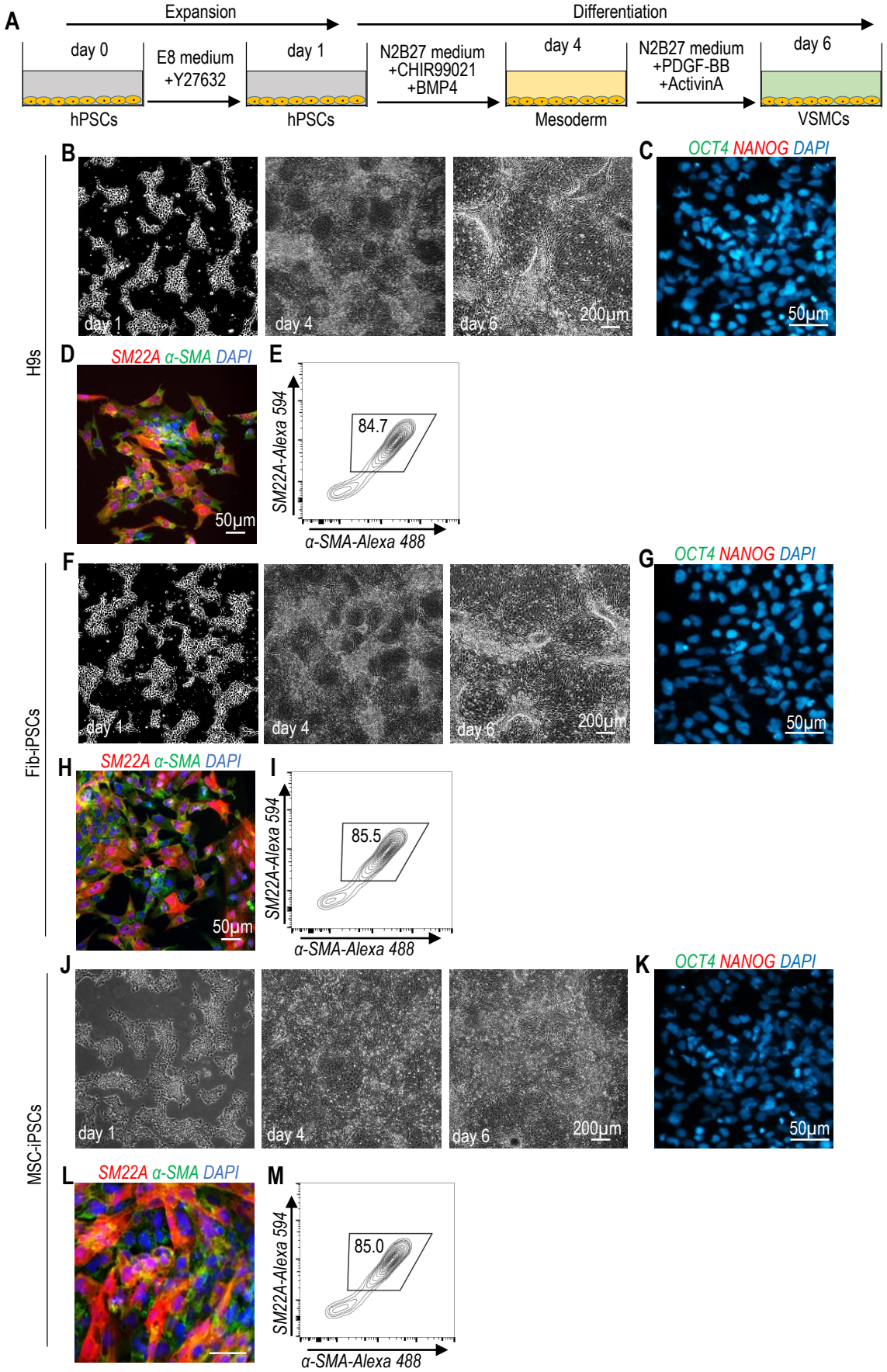

Figure S2. Differentiate hPSCs (H9s, Fib-iPSCs and MSC-iPSCs) into VSMCs in 2D cultures.
(**A**) Illustration of the VSMC differentiation protocol in 2D cultures.
(**B, F, J**) Phase images of day 1, 4 and 6 cells during VSMC differentiation. Scale bar, 200 μm.
(**C, G, K**) Immunostaining of day 6 cells for hPSCs markers, *OCT4* and *NANOG*. Scale bar, 50 μm.
(**D, H, L**) Immunostaining of day 6 cells for VSMC markers, *SM22A* and *α-SMA*. Scale bar, 50 μm.
(**E, I, M**) Flow cytometry analysis of day 6 hPSC-VSMCs for *SM22A* and *α-SMA*.

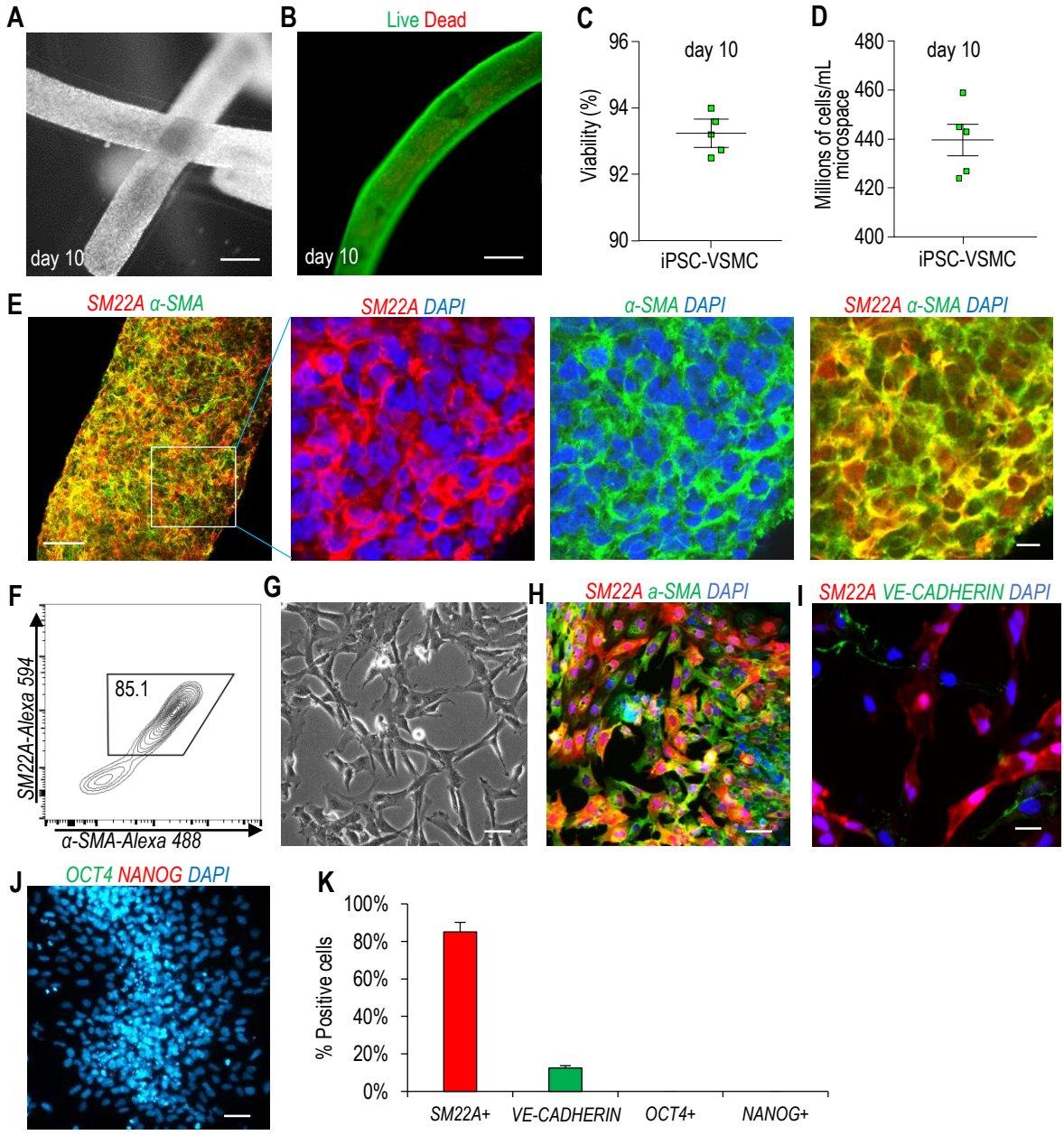

Figure S3. Differentiating Fib-iPSCs into VSMCs in alginate hydrogel tubes.
(**A**) Phase images of day 10 cells. Scale bar, 200 µm.
(**B, C**) Live/dead staining and cell viability analysis of day 10 cells. Data are represented as mean ± SD (n=5). Scale bar, 200 µm.
(**D**) Volumetric yield on day 10. Data are represented as mean ± SD (n=5).
(**E, F**) Immunostaining and flow cytometry analysis of VSMC markers *SM22A* and *α-SMA* on day 10 cells. Scale bar, 50 µm and 10 µm.
(**G-K**) The day 10 cell masses were dissociated into single cells and plated on 2D surface overnight. Phase image (**G**), immunostaining showed majority of the cells were *SM22A+/α-SMA+* (**H**), and ~10% *VE-CADHERIN+* endothelial cells (**I, K**), but no *OCT4+/NANOG+* undifferentiated Fib-iPSCs (**J, K**). Data are represented as mean ± SD (n=3). Scale bar, 50 µm.

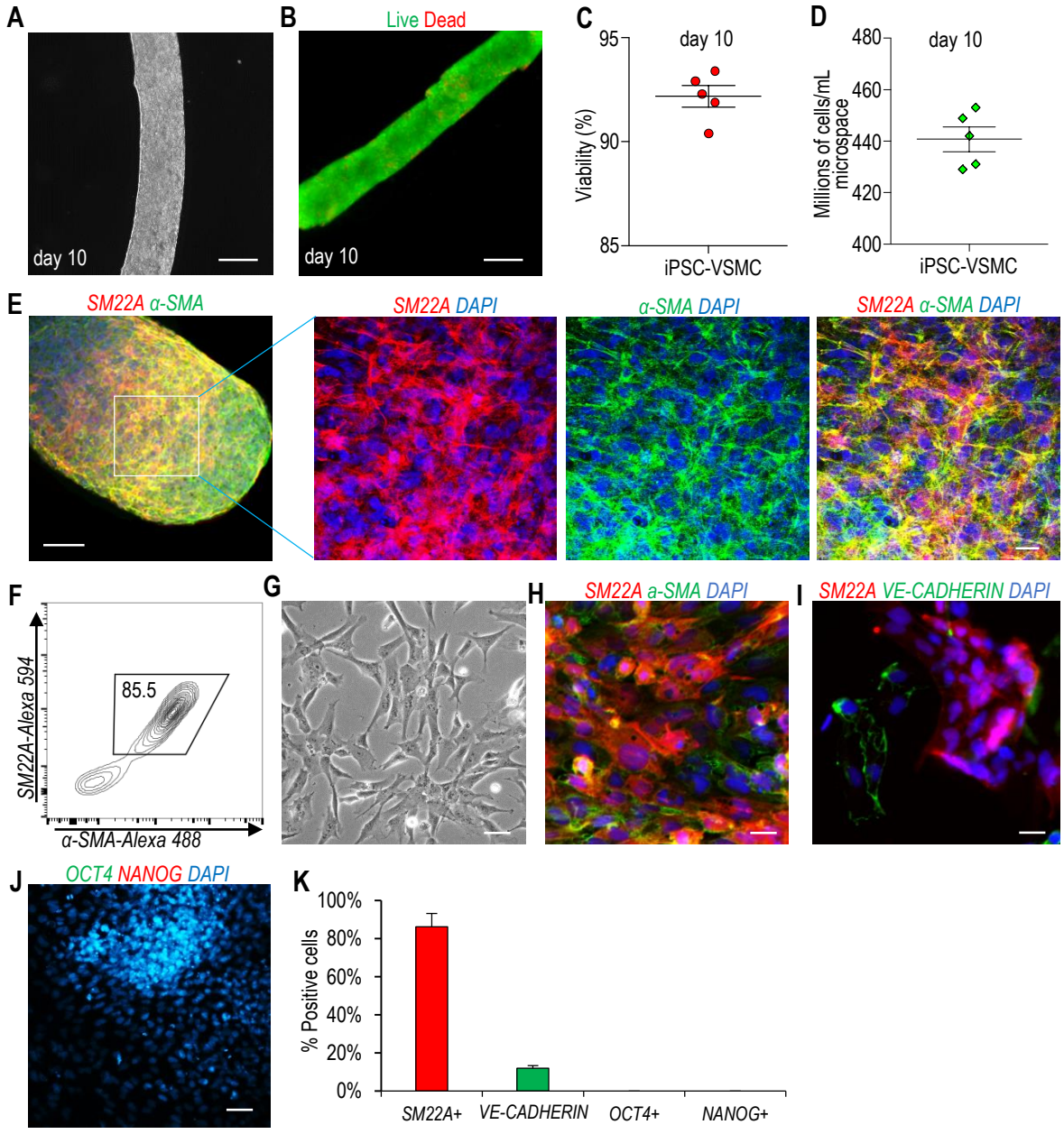

Figure S4. Differentiating MSC-iPSCs into VSMCs in alginate hydrogel tubes.
(**A**) Phase images of day 10 cells. Scale bar, 200 μm.
(**B, C**) Live/dead staining and cell viability analysis of day 10 cells. Data are represented as mean ± SD (n=5). Scale bar, 200 μm.
(**D**) Volumetric yield on day 10. Data are represented as mean ± SD (n=5).
(**E, F**) Immunostaining and flow cytometry analysis of VSMC markers *SM22A* and *α-SMA* on day 10 cells. Scale bar, 50 μm and 10 μm.
(**G-K**) The day 10 cell masses were dissociated into single cells and plated on 2D surface overnight. Phase image (**G**), immunostaining showed majority of the cells were *SM22A+/α-SMA+* (**H**), and ~10% *VE-CADHERIN+* endothelial cells (**I, K**), but no *OCT4+/NANOG+* undifferentiated MSC-iPSCs (**J, K**). Data are represented as mean ± SD (n=3). Scale bar, 50 μm and 20 μm.

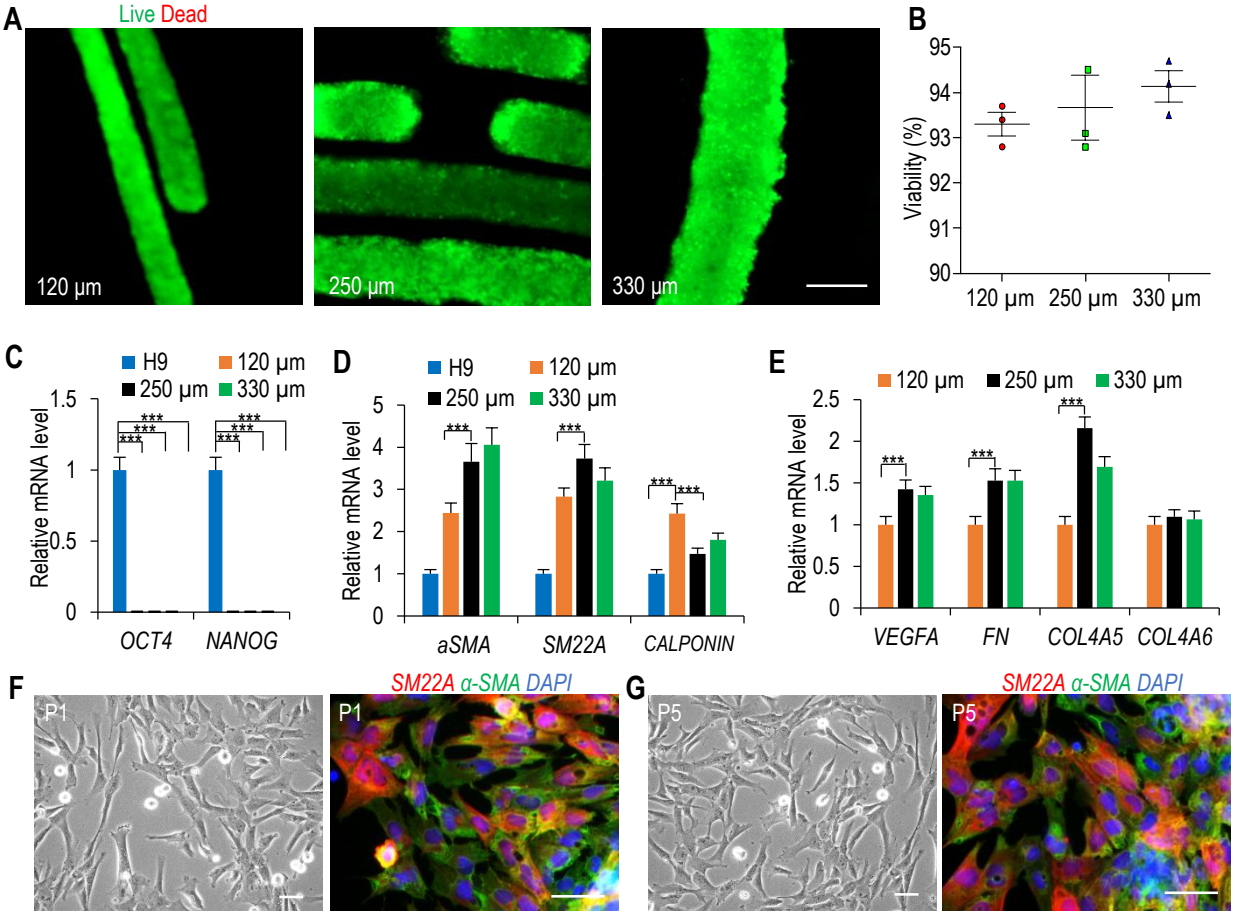

Figure S5. Effect of hydrogel tube diameter on VSMC differentiation.
(**A, B**) Live/dead staining and cell viability analysis of day 10 hPSC-VSMCs. Data are represented as mean ± SD (n=3). Scale bar, 200 μm.
(**C-E**) qRT-PCR analysis of gene expression of H9s and day 10 hPSC-VSMCs in 120 μm, 250 μm and 330 μm hydrogel tubes, including pluripotency markers *OCT4* and *NANOG*, VSMC markers *α-SMA, SM22A* and *CALPONIN*, growth factor *VEGFA*, and extracellular matrices *FN, COL4A5* and *COL4A6*. Data are represented as mean ± SD (n=3). ****p*<0.001.
(**F, G**) Phase and immunostaining images of VSMCs at passage 1 (P1) and 5 (P5) after bioreactor-VSMCs were plated on 2D plates. Scale bar, 50 μm.

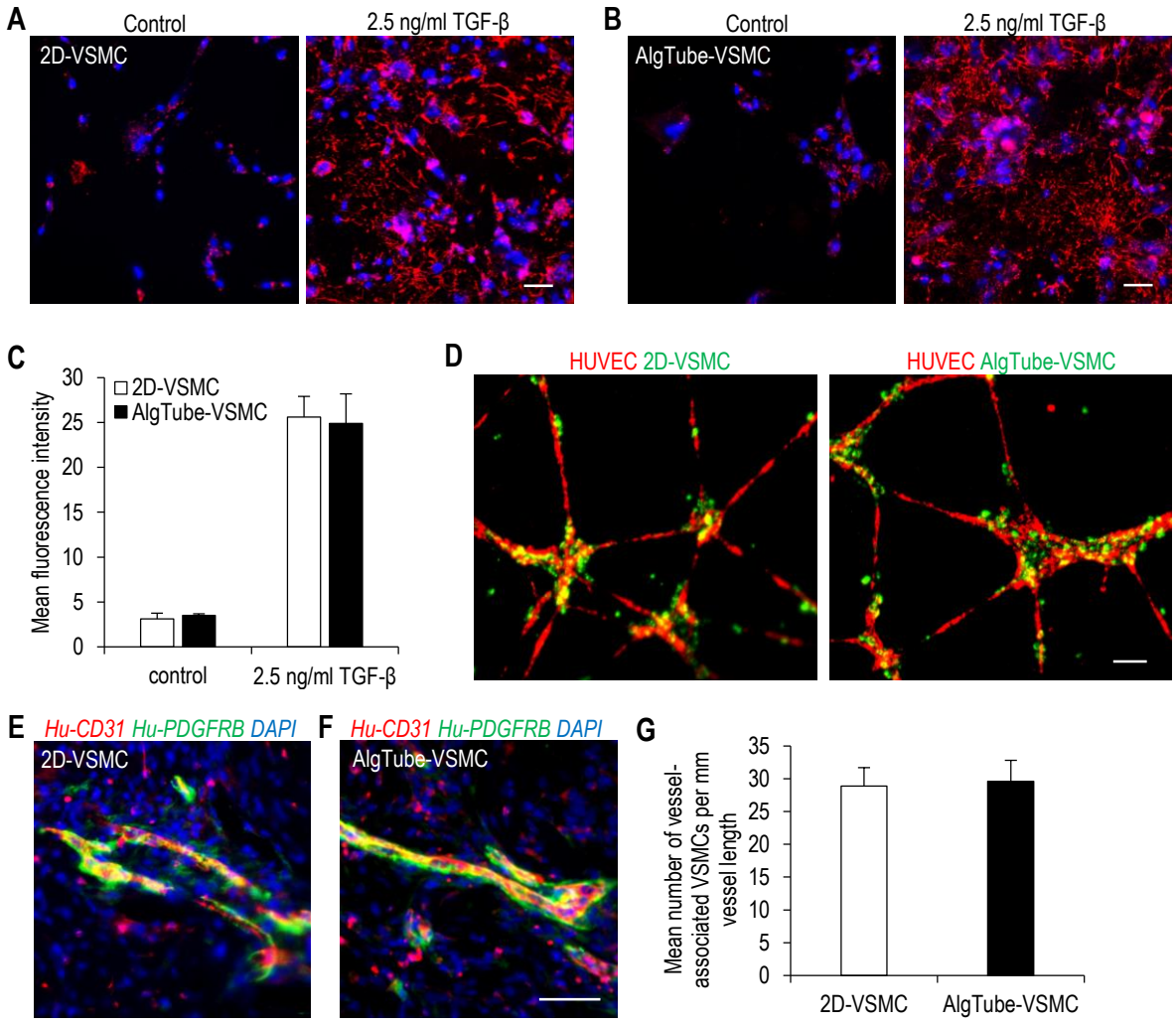

Figure S6. Properties of VSMCs derived from Fib-iPSCs in 2D (2D-VSMCs) and alginate hydrogel tubes (AlgTube-VSMCs).
(**A-C**) Fibronectin production after 24 hours of 2.5 ng/mL TGF-β treatment. Data are represented as mean ± SD (n=3). Scale bar, 50 μm.
(**D**) Co-culture of VSMCs and HUVECs. Scale bar, 50 μm.
(**E, F**) When VSMCs and HUVECs were co-transplanted subcutaneously, 2D-VSMCs (**E**) and AlgTube-VSMCs (**F**) formed nice vascular structures. Scale bar, 50 μm.
(**G**) 2D-VSMCs and AlgTube-VSMCs showed similar number of VSMCs attached to vessel.

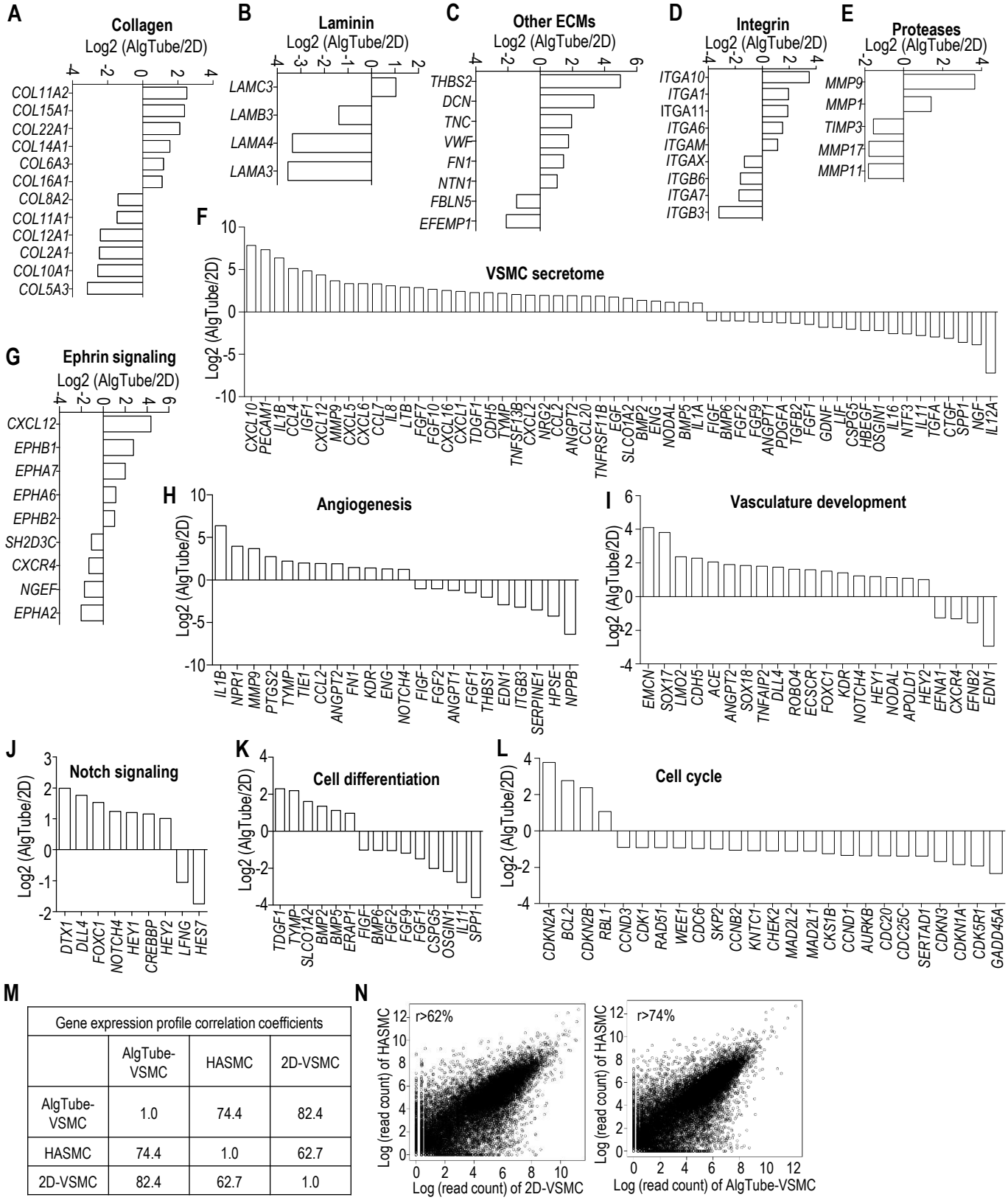

Gene expression profile correlation coefficients			
	AlgTube-VSMC	HASMC	2D-VSMC
AlgTube-VSMC	1.0	74.4	82.4
HASMC	74.4	1.0	62.7
2D-VSMC	82.4	62.7	1.0

Figure S7. Differential gene expression analysis of H9s, AlgTube-VSMCs and 2D-VSMCs derived from H9s. (**A-L**) Log2 (expression level in AlgTube-VSMCs/expression level in 2D-VSMCs) analysis of genes related to extracellular matrices (**A-E**), VSMC secretome (**F**), Ephrin signaling (**G**), angiogenesis (**H**), vasculature development (**I**), Notch signaling (**J**), cell differentiation (**K**) and cell cycle (**L**). (**M, N**) The global gene expression correlation coefficients (**M**) and scatter plot in log scale (**N**) of gene expression between AlgTube-VSMCs or 2D-VSMCs and HASMCs.

Table S1. Antibodies used in this study (Related to Figure 1, 2, 3, 6 and Figure S1-6).

Antibody	Supplier	Catalog. No	Species	Dilution
VE-Cadherin	Santa Cruz	sc-9989	Mouse	1:100 (IF&FC)
α-SMA	Santa Cruz	sc-130616	Mouse	1:100 (IF&FC)
SM22A	Abcam	ab14106	Rabbit	1:100 (IF&FC)
SSEA4	R&D System	962648	Mouse	1:200 (IF&FC)
ALP	R&D System	962647	Mouse	1:200 (IF&FC)
HNF-3β	Santa Cruz	sc-101060	Mouse	1:200 (IF)
OCT4	R&D System	962649	Goat	1:200 (IF&FC)
NANOG	R&D System	963488	Goat	1:200 (IF&FC)
NESTIN	BioLegend	809801	Mouse	1:500 (IF&FC)
Fibronectin	Abcam	ab2413	Rabbit	1:500 (IF)
Human-PDGFRB	ThermoFisher	PA5-14718	Rabbit	1:100 (IF)
Human-CD31	BD Biosciences	555444	Mouse	1:200
Secondary antibody	Jackson ImmunoResearch	715-545-151	Donkey	1:500
Secondary antibody	Jackson ImmunoResearch	711-585-152	Donkey	1:500
Secondary antibody	Jackson ImmunoResearch	711-165-152	Donkey	1:500
Secondary antibody	Jackson ImmunoResearch	705-605-147	Donkey	1:500

Table S2. Real time qPCR primers used in this study (Related to Figure 3, 6 and Figure S3).

Primer Name	**Forward 5'-3'**	**Reverse 5'-3'**
SM22A	TGAAGGCGGCTGAGGACTAT	TCTGTTGCTGCCCATCTGAA
α-SMA	CTGGGACGACATGGAAAA	ACATGGCTGGGACATTGA
Calponin	AGCATGGCGAAGACGAAAGGAA	CCCATCTGCAGGCTGACATTGA
SMTN	CGGCCTGCGCGTGTCTAATCC	CTGTGACCTCCAGCAGCTTCCGAA
Elastin	CAGCTAAATACGGTGCTGCTG	AATCCGAAGCCAGGTCTTG
MYH11	AGATGGTTCTGAGGAGGAAACG	AAAACTGTAGAAAGTTGCTTATTCACT
MMP9	GCTTTTCTTCTTCTCTGGGCGCC	CGGTCCTGGCAGAAATAGGCTTT
VEGFA	TCACAGGTACAGGGATGAGGACAC	TCCTGGGCAACTCAGAAGCA
VEGFB	GCTTAGAGCTCAACCCAGACACC	CAAGTCACCCTGCTGAGTCTGAA
VEGFC	CAGCACGAGCTACCTCAGCAAG	TTTAGACATGCATCGGCAGGAA
Fibronectin	GCACCACAGCCATCTCACAT	TCCAACGGCCTACAGAATTT
Collagen4A5	AAAAGAGCCCACGGTCAAG	GGGGTAGAGAGCCAGTAAGAA
Collagen4A6	ACCCTGCTGAGATCTGCTGT	GGCCCATCAAATCTTTCTGA
PECAM1	GCAGCATCGTGGTCAACATAA	GCAGGACAGGTTCAGTCTTTCA
ANGPT2	ACCCCACTGTTGCTAAAGAAGA	CCATCCTCACGTCGCTGAATA
NOTCH4	CCTGGCTCCTTCAACTGCC	GCAAGTAGGTCCAGACAGGT
DLL4	GTCTCCACGCCGGTATTGG	CAGGTGAAATTGAAGGGCAGT
OCT4	CCCCAGGGCCCCATTTTGGTACC	ACCTCAGTTTGAATGCATGGGAGAGC
NANOG	TACCTCAGCCTCCAGCAGAT	CCTTCTGCGTCACACCATT
GAPDH	TCGACAGTCAGCCGCATCTTCTTT	ACCAAATCCGTTGACTCCGACCTT

Supplemental Experimental Procedures

Routine Cell Culture

H9 hESCs (#WA09, WiCell) were purchased from WiCell Research Institute. Fib-iPSCs and MSC-iPSCs reprogrammed from fibroblasts and mesenchymal stem cells, respectively, were obtained from Human Embryonic Stem cell core, Harvard Medical School and have well characterized and described in the literature(Park et al., 2008). hPSCs (H9s and iPSCs) were maintained in 6-welll plate coated with Matrigel in Essential 8^{TM} medium. Cells were passaged every 4 days with 0.5 mM EDTA. Medium was changed daily. Cells were routinely checked for the expression of pluripotency markers, OCT4 and NANOG, their capability to form teratomas in immunodeficient mice, their karyotypes, and bacterial or mycoplasma contamination. HUVECs (#00191027, Lonza) were obtained from Lonza.

Processing Alginate Hydrogel Tubes

A custom-made micro-extruder was used to process the alginate tubes according to our previous publication(Li et al., 2018a). Briefly, a hyaluronic acid (HA) solution containing single cells and an alginate solution was pumped into the central and side channel of the home-made micro-extruder, respectively, and extruded into a $CaCl_2$ buffer (100 mM) to make alginate hydrogel tubes. Subsequently, $CaCl_2$ buffer was replaced by cell culture medium. We made the hydrogel tubes with diameter of 120, 250 and 330 μm and found 250 μm was optimal for cell culture. We decided to use 250 μm hydrogel tubes with 40 μm shell thickness for all the cell culture studies. To make these tubes, the flow rates for the cell suspension and alginate solution were 30 μL/min and 30 μL/min, respectively.

Culturing hPSCs in Alginate Hydrogel Tubes

For a typical cell culture, 20 μL cell solution in alginate hydrogel tubes were suspended in 3 mL E8 medium with 10 μM ROCK inhibitor in a 6-well plate and cultured in an incubator with 5% CO_2, 21% O_2 at 37 °C. Medium was changed daily. To passage cells, medium was removed, and alginate hydrogels were dissolved with 0.5 mM EDTA for 5 minutes. Cell masses were collected by centrifuging at 100 g for 5 minutes, and treated with Accutase at 37 ºC for 10 minutes and dissociated into single cells if needed.

Making hPSC-VSMCs in 2D Culturing or Alginate Hydrogel Tubes

For VSMCs differentiation in 2D, hPSCs were dissociated with Accutase and plated on Matrigel-coated plate at a density of 40,000 cells/cm^2 in E8 medium with 10 μM ROCK inhibitor. After 24 hours, the medium was replaced with differentiation medium, consisting of N2B27 medium (1:1 mixture of DMEM/F12 (#SH30004.04, HyClone) with Glutamax-I (#35050061, Life Technologies) and Neurobasal medium (#21103049, Life Technologies) supplemented with N2 (#17502048, Life Technologies) and B27 minus vitamin A (#12587010, Life Technologies) with 8 μM CHIR99021 (#C6556, LC laboratories) and 25 ng/mL BMP4 (#314BP010, R&D Systems). After 3 days, the differentiation medium was replaced by VSMC induction medium consisting of N2B27 medium supplemented with 10 ng/mL PDGF-BB (#100-14B, PeproTech) and 2 ng/mL ActivinA (#338-AC, R&D Systems). The medium was exchanged every day. VSMCs were harvested for analysis on day 6.

For VSMCs differentiation in AlgTubes, single hPSCs were encapsulated in AlgTube ($1.0x10^6$ cells/mL) and cultured in E8 medium for 5 days. E8 medium was removed and replaced with VSMC differentiation medium. After 3 days, the differentiation medium was replaced by VSMC induction medium. The induction medium was changed after 1 day. On day 10, cell masses were collected for following analysis.

Producing hPSC-VSMCs in Alginate Hydrogel Tubes in the Prototype Bioreactor

1 mL of hPSCs solution in AlgTube were suspended in a bioreactor. hPSCs were cultured in E8 medium with 5% CO_2, 21% O_2 at 37 °C for 5 days. E8 medium was removed and replaced with VSMC differentiation medium for 3 days, followed by VSMC induction medium for 2 days. For bioreactor, medium was stored in a bellow bottle that was periodically pressed to flow the medium into, or released to withdraw the medium from bioreactor. On day 10, hydrogel tubes were dissolved by adding 0.5 mM EDTA buffer. Cell masses were pelleted by centrifugation. Cell masses were dissociated into single cells through incubating in Accutase at 37 °C for 10 minutes. Magnetic beads coated with anti-CD144 antibodies were added to remove CD144+ hPSC-ECs with a magnetic cell separator. The bioprocess was repeated 2 times.

Immunocytochemistry and Flow Cytometry

For 2D immunostaining, the 2D cells were fixed with 4% paraformaldehyde (PFA) at room temperature for 20 minutes, permeabilized with 0.25% Triton X-100 for 30 minutes, and blocked with 5% donkey serum for 1 hour before incubating with primary antibodies (**Table S1**) at 4 °C overnight. After extensive washing, secondary antibodies (**Table S1**) and 10 µM 4', 6-Diamidino-2-Phenylindole (DAPI) in 2% BSA were added and incubated at room temperature for 4 hours. Cells were washed with PBS for 3 times before imaging with A1 confocal microscope. For cell mass immunostaining, after fixation for 30 minutes, cell masses were incubated with PBS + 0.25% Triton X-100 + 5% (vol/vol) goat serum + primary antibodies at 4 °C for 48 hours. After extensive washing, secondary antibodies in 2% BSA were added and incubated at 4 °C for 24 hours. Cells were washed with PBS three times before imaging with a confocal microscope.

For flow cytometry analysis, the harvested cells were dissociated into single cells with Accutase, then fixed with 4% PFA at room temperature for 20 minutes. Single cells were stained with primary antibodies (**Table S1**) at 4 °C overnight. After washing 3 times with 1% BSA in PBS, secondary antibodies were added and incubated at room temperature for 2 hours. Cells were washed with 1% BSA in PBS and analyzed using a Cytek DxP10 flow cytometer. Single-color and isotype controls were used for compensation and negative gating.

RNA Extraction, cDNA Synthesis and Quantitative PCR

Total RNAs for qPCR and RNA sequencing were extracted from undifferentiated hPSCs, 2D-VSMCs and AlgTube-VSMCs on day 5 of the differentiation using Trizol (#15596018, Invitrogen), according to the manufacturer's instructions. Reverse transcription was done with the Maxima First Strand cDNA Synthesis Kit (#K1642, Life Technologies). Quantitative real-time PCR was carried out in an Eppendorf MasterCycler RealPlex4 (ThermoFisher Scientific) using the Power SYBR Green PCR Master Mix (#4367659,

ThermoFisher), according to the manufacturer's instructions. The data were normalized to the endogenous GAPDH. Primer sequences are listed in **Table S2**.

Embryoid Body (EB) Differentiation

hPSCs were suspended in DMEM + 20% FBS + 10 μM β-mercaptoethanol in low adhesion plate for 6 days. The cell masses were then transferred into plates coated with 0.1% gelatin and cultured in the same medium for another 6 days, followed by fixation and staining as described above.

Teratoma Formation *in vivo*

The animal experiments were carried out following the protocols approved by the University of Nebraska–Lincoln Animal Care and Use Committee. $1.0x10^6$ hPSCs were suspended in 25 μL PBS + 25 μL Matrigel and injected subcutaneously at the back of the neck of the NOD-SCID mice (female, age 7 weeks, Charles River Laboratory). Three mice (two teratomas per mouse) were used for teratoma assay for each hPSC line. Teratomas were harvested when their size reached 2 cm. Teratomas were fixed with 4% PFA for 48 hours, dehydrated with 70%, 95% and 100% ethanol sequentially, and de-fated with xylene for 2 hours before being embedded in paraffin. 10 μm thick sections were cut and stained with hematoxylin and eosin. The structures from all 3 germ layers were identified by a trained specialist.

Co-Culture Assay of HUVECs and hPSC-VSMCs

200 μL of Matrigel was added into each well of a 12-well plate and incubated for 30 minutes at 37 °C to allow the formation of a thin layer of hydrogel. For the functional tube formation and association assays *in vitro*, the HUVECs and the hPSC-VSMCs were prestained with DiI (red) and DiO (green), respectively, according to the manufacturer's instructions. Cells were grown in EGM-2 medium supplemented with 50 ng/mL VEGF-A. For the experiment, $2.0x10^4$ HUVECs/cm^2 and $2.0x10^4$ hPSC-VSMCs/cm^2 were co-cultured for 24 hours in the incubator. Cells were fixed with 2% PFA for 10 minutes and analyzed using Zeiss fluorescence microscope.

Fibronectin Production

After 5 days of differentiation, 2D-VSMCs and AlgTube-VSMC were seeded in N2B27 containing 10 ng/mL PDGF-BB at 40,000 cells/cm^2 on gelatin-coated wells. After 24 hours, the medium was changed to N2B27 with 10 ng/mL PDGF-BB supplemented with DMSO or 2.5 ng/mL TGF-β. After 24 hours, cells were washed with PBS, fixed with 4% PFA for 10 min at room temperature, and immunofluorescence staining of deposited Fibronectin was performed (**Table S1**).

Contraction Study

2D-VSMCs and AlgTube-VSMCs were seeded in N2B27 containing 2 ng/mL ActivinA and 2 μg/mL at 40,000 cells/cm^2 on Collagen-coated wells according to previous studies(Matsumoto et al., 2007; Patsch et al., 2015). After 48 hours, they were stained with 2.5 μM Fluo-4 AM (#50018, Biotium) at 37 °C for 1 hour. Contraction was induced by treating the cells with 100 μM carbachol (#2810, Tocris). Contraction images of VSMCs were acquired by a Zeiss fluorescence microscope. The fluorescence intensity of

intracellular calcium flux, cell surface area (mm^2) and percent change of cell surface area was assessed by ImageJ software.

Matrigel Plug Assay

Animal procedures were performed in accordance with an IACUC-approved protocol reviewed by the University of Nebraska–Lincoln Animal Care and Use Committee. 6-8 week old female SCID mice (Charles River Laboratory) were used. HUVECs and hPSC-VSMCs were added to the Matrigel mixture to a final concentration of 10 million cells/mL. The Matrigel mixture (300 µL) was then immediately engrafted subcutaneously into the dorsal flank of the mouse. Two implants were engrafted per animal. Implants were recovered after 14 days, then the implants were excised. They were fixed in 4% PFA. Hematoxylin & eosin staining, and immunostaining was performed to analyze the tube formation potential *in vivo*. Six mice were used for the Matrigel plug assay. Mean number of vessel-associated VSMCs per mm vessel length was assessed by ImageJ software.

RNA Sequencing and Data Analysis

Total RNA of day 6 VSMCs from 2D culture and day 10 VSMCs from AlgTubes (note: both VSMCs were differentiated for 5 days) were prepared with RNeasy mini kit (cat # 74104 QIAGEN) according to the manufacturer's instruction. Prior to RNA sequencing, magnetic beads coated with anti-CD144 antibodies were added to remove CD144+ hPSC-ECs with a magnetic cell separator. VSMCs reached 95% purity after purification. Libraries were prepared with TruSeq Stranded mRNA Library Prep Kit and sequenced with Illumina NextSeq 500. 20 million 75 bp paired-end reads were generated for each sample. The thresholds for differential expression were set at fold-change > 2 and adjusted P-values < 0.001 for the null hypothesis. Methods for the data processing, heatmap generating, PCA analysis, differential gene expression analysis have been described in our previous publication(Li et al., 2018a).

Statistical Analysis

The data are presented as the mean ± standard deviation (SD) from three independent experiments. We used an unpaired t-test to compare two groups and one-way ANOVA to compare more than two groups. A sample size of 3 was selected so that at a significance level of 0.05 there was at least 95% chance of detecting two SD's difference in outcome between the groups. All data were processed using GraphPad Prism 7 (GraphPad Software, Inc., La Jolla, CA).

Data Availability

The final processed data and raw fastq files were submitted to Gene Expression Omnibus (GEO) with the accession number GSE99776 and GSE109683. All other data supporting the findings of this study are available within the paper and its Supplemental Information.

References

Park, I.H., Zhao, R., West, J. a., Yabuuchi, A., Huo, H., Ince, T. a., Lerou, P.H., Lensch, M.W., and Daley, G.Q. (2008). Reprogramming of human somatic cells to pluripotency with defined factors. Nature *451*, 141–146.

Li, Q., Lin, H., Du, Q., Liu, K., Wang, O., Evans, C.A., Christian, H.M., Zhang, C., and Yuguo, L. (2018a). Scalable and physiologically relevant microenvironments for human pluripotent stem cell expansion and differentiation. Biofabrication *10*, 025006.

Matsumoto, H., Moir, L.M., Oliver, B.G.G., Burgess, J.K., Roth, M., Black, J.L., and McParland, B.E. (2007). Comparison of gel contraction mediated by airway smooth muscle cells from patients with and without asthma. Thorax *62*, 848–854.

Patsch, C., Challet-Meylan, L., Thoma, E.C., Urich, E., Heckel, T., O'Sullivan, J.F., Grainger, S.J., Kapp, F.G., Sun, L., Christensen, K., et al. (2015). Generation of vascular endothelial and smooth muscle cells from human pluripotent stem cells. Nat. Cell Biol. *17*, 994–1003.